THE FLORIDA STATE UNIVERSITY

COLLEGE OF ARTS AND SCIENCES

SEA BREEZE VARIATIONS OF FLORIDA

By

LAUREN MOELLER

A Thesis submitted to the
Department of Meteorology
in partial fulfillment of the
requirements for the degree of
Master of Science

Degree Awarded:
Summer Semester, 2011

The members of the committee approve the thesis of Lauren Moeller defended on March 31, 2011.

_____
Vasubandhu Misra
Professor Directing Thesis

_____
James J. O'Brien
Professor Co-Directing Thesis

_____
Henry Fuelberg
Committee Member

_____
Mark Bourassa
Committee Member

The Graduate School has verified and approved the above-named committee

My thesis and my work are dedicated to my wonderful parents, Larry and Kim, my sisters Kayla and Jenna, my brother Brandon, and most of all, my support and love, my fiancé Chris.

ACKNOWLEDGEMENTS

First of all I would like to thank Dr. Vasu Misra for accepting me as one of his students here at FSU, and giving me the opportunity to do this work. He has continually pushed me to do the best that I can, and I would not have accomplished as much as I have without his direction and advice.

I would also like to thank Dr. Mark Bourassa, Dr. Henry Fuelberg (HEF), and especially Dr. James J. O'Brien for serving on my committee. Your advice and guidance were extremely helpful from the get-go, and my work here has improved due to your thoughtful contributions.

Along with the committee I would like to thank Dr. Steven Chan and Dr. Lydia Stefanova for their guidance and support, and for helping me through any scripting trouble.

Next I want to thank my family for their continuous support even when they were hundreds of miles away. You guys believed in me during the toughest of times, and this could not have happened without you!

My friends have also been an invaluable support during my time here at FSU. An extra special shout-out goes to those at COAPS and those in Dr. Misra's lab. You guys have made these last two years some of the best in my life, and whether it was a shoulder to cry on or some great advice, you all had it ready. Thank you!

Finally, I want to thank my fiancé Chris for his love and support throughout my graduate school career. There are no words to describe my gratitude for all that you do for me.

TABLE OF CONTENTS

LIST OF TABLES

LIST OF FIGURES

ABSTRACT

This study investigates the variations of the sea breeze both diurnally and interannually. The region of focus is along the panhandle of Florida in the boreal summer season, primarily along the 30.5°N latitude. To examine diurnal differences, a climatology of the sea breeze cross-sections is calculated eight times daily between the years 1979 and 2001. This is done using very high resolution (10 km) dynamically downscaled analyses from the NCEP-DOE (R2) and the ECMWF ERA-40 for the southeast US. This high resolution downscaled product is validated with other independent observations to show fidelity. Results from these diurnal analyses show that the sea breeze as well as the precipitation peaks at 4pm.

Using the same model data, other composites are made based on the size of the Atlantic Warm Pool (AWP) to analyze sea breeze variations over an interannual time scale. The size of the AWP is related to the subtropical high, which undergoes an eastward shift and a decrease in intensity for large AWP years. This leads to a more cyclonic large-scale low-level flow for these particular years. This study finds that this synoptic flow pattern will suppress the sea breeze circulation and lessen precipitation amounts over the panhandle region.

CHAPTER ONE

INTRODUCTION

1.1 Objective and Motivation

The purpose of this study is to determine whether low-frequency variations of the sea breeze in Florida exist, and if they do, to examine a possible cause of these variations. The hypothesis is that the sea breeze does have low-frequency variations. Previous studies, have often examined sea breezes as individual events, or they have focused on the disparities of the sea breeze circulation that can occur daily. However, this study concentrates on the interannual variations of the sea breeze, a topic that has not yet been published. These low-frequency variations are examined with respect to changes in the Atlantic Warm Pool (AWP), which have been studied only since 2001. The findings of this study will provide another extensive teleconnection associated with the AWP (Wang and Enfield 2001; Wang et al. 2006; Wang et al. 2008). In addition, determining the low-frequency variation of the sea breeze in Florida will assist the agricultural community, long-range forecasting decisions, and model assessment. A paper written by Carter (2003) stressed the importance of low frequency variability to the agricultural community in the southeast. Long-range climate models have differing opinions on the amount of precipitation the region will receive and what temperature trends to expect. Therefore it is important to establish all possible teleconnections that can effect the weather of this region; this knowledge will then drive to improve climate models (Carter 2003). Forecasters will also benefit from this knowledge, as shown by Powell and Rinard (1998).

1.2 Background

1.2.1 Definition of the Sea Breeze

The sea breeze is part of a thermal circulation that exists because of differential heating between the land and the water (Biggs and Graves 1962; Simpson 1994). Temperatures over land increase and decrease more dramatically than those over the water; a pressure gradient is created since higher pressure exists over the water surface during the daytime. This process induces a flow from higher pressure over the water to relatively lower pressure over land, which is known as a sea breeze (Fig. 1.1). The opposite occurs at night and a land breeze develops; however, the land breeze is less prominent than its daytime counterpart (Mak and Walsh 1976).

The thermal circulation is also more prominent in the summer for the Northern Hemisphere because the temperature gradient between the land and water is at its highest (Simpson 1994).

Sea breezes are especially important during Florida summers (Pielke 1974) because they are responsible for the precipitation critical to agricultural interests.

Pielke's 1974 study was one of the first to use a 3D model to simulate the sea breeze along the Florida peninsula; prior studies (Estoque 1962; Hsu 1970; Neumann and Mahrer 1971) used a 2D theoretical model. The 3D model showed two sea breezes forming, one along each coast of the Florida peninsula. Pielke juxtaposed vertical velocity predictions and composite radar reflectivities for multiple days and found that for synoptically quiescent days the sea breeze was the main instigator of convection in Florida during the summer months.

1.2.2 Synoptic Scale Influences

Even though a sea breeze is a mesoscale feature, it is often influenced by forcing that exists on a synoptic scale. The synoptic influences were first demonstrated by Lopez et al. (1984), who classified the amount of convective coverage into four categories on the basis of the radar data for each day in south Florida. The average synoptic pattern was then produced for each category by using soundings and maps. They discovered that the synoptic flow regimes' influence on the sea breeze circulations was the greatest contributor to the differences between the convective categories. In a follow-up study, Blanchard and Lopez (1985) showed that the patterns of convection on the radar were closely related to the synoptic wind field.

Arritt (1993) demonstrated how the background synoptic wind flow influences the sea breeze by simulating, in a 2D model, different ambient offshore and onshore flows. The strength and direction of the ambient flow greatly influenced the strength and inland penetration of the sea breeze. For example, if light to moderate offshore flow existed, the sea breeze front was enhanced and able to penetrate inland. Arritt also discovered that if the offshore flow were too strong, the sea breeze could develop, but it would stay mainly offshore. The offshore and onshore flow can weaken or strengthen the temperature gradient between the land and sea. Background synoptic winds also influence the advection of moisture, as demonstrated by Fuelberg and Biggar (1994) when they examined the convection occurring along the Florida panhandle.

Since the synoptic flow has such an influence on the sea breeze, an analysis of the prevailing synoptic conditions is necessary for sea breeze forecasting. Powell and Rinard (1996)

described the process of forecasting the sea breeze and convection during the 1996 Summer Olympic Games in Atlanta, Georgia. Figure 1.2, from Powell and Rinard (1996), shows the different synoptic regimes that occurred during the summer of 1996 with respect to the Bermuda high (also known as the North Atlantic subtropical high) and pressure systems moving through the United States. Each regime resulted in a different background flow in the forecast region of Georgia. Additional studies also concluded that the location of the Bermuda high influences the formation of the sea breeze (Lopez et al. 1984; Blanchard and Lopez 1985). A study by Miller and Keim (2003) determined which synoptic patterns were conducive for sea breeze formation in an attempt to develop a forecasting product for sea breezes.

The synoptic scale influences on sea breezes have been well documented. The present study argues that since the synoptic flow varies interannually, low-frequency variations of the sea breeze in Florida exist. These low-frequency variations will be analyzed in the context of the AWP.

1.2.3 The Atlantic Warm Pool

The AWP was defined in Wang and Enfield (2001) as a region in the Gulf of Mexico, the Caribbean Sea, and the western tropical North Atlantic that has sea temperatures of at least 28.5°C. The size of the AWP fluctuates from year to year, as shown in a schematic by Wang et al. (2006) (Fig. 1.3). For large AWP years, the 28.5°C isotherm dips east and south to reach into the tropical North Atlantic, and in the small AWP years the AWP is confined to the Gulf of Mexico and parts of the Caribbean Sea. On average, the large AWP is three times larger than the small AWP. Climatologically, the AWP is largest during the later part of the warm season (August, October, November; Wang et al. 2006), but the AWP is distinguishable during June and July as well. Wang et al. (2006) also noted that the variability of the AWP size was unrelated to the El-Niño Southern Oscillation (ENSO) two-thirds of the time, but ENSO can influence the AWP. However, this study is limited to the AWP effects on the sea breeze and does not address the possible impacts of ENSO on the AWP.

Various teleconnections have been discussed in the literature in response to the implications of the different sizes of the AWP (Wang et al. 2006; Wang et al. 2008). During large AWP years, the pressure falls in the Caribbean region and Mexico and the precipitation increases. Wind magnitude decreases for large AWP years over the Gulf of Mexico, thus creating a weaker Great Plains low-level jet (GPLLJ). This in turn creates an environment for

reduced precipitation over the Great Plains region due to lack of transport. Work has also been done to relate the size of the AWP to Atlantic hurricane activity (Wang et al. 2006; Wang and Lee 2007; Wang et al. 2008). For large AWP years the Caribbean low-level jet (CLLJ) weakens because of the position of the Bermuda high, reducing the vertical wind shear over the Caribbean region. In conjunction with lower values of vertical wind shear, warmer waters extend farther to the east and south than they normally would for small AWP years. It has been shown that there is increased hurricane activity in the Atlantic basin for large AWP years because of the lower wind shear and warmer waters.

This study focuses on the AWP teleconnections and how they modulate the sea breeze in Florida on an interannual time scale. The remainder of this paper is organized as follows: the model runs, verification data, and methodology are described in chapter two; the model results are presented and discussed in depth in chapter three; and conclusions are stated in chapter four.

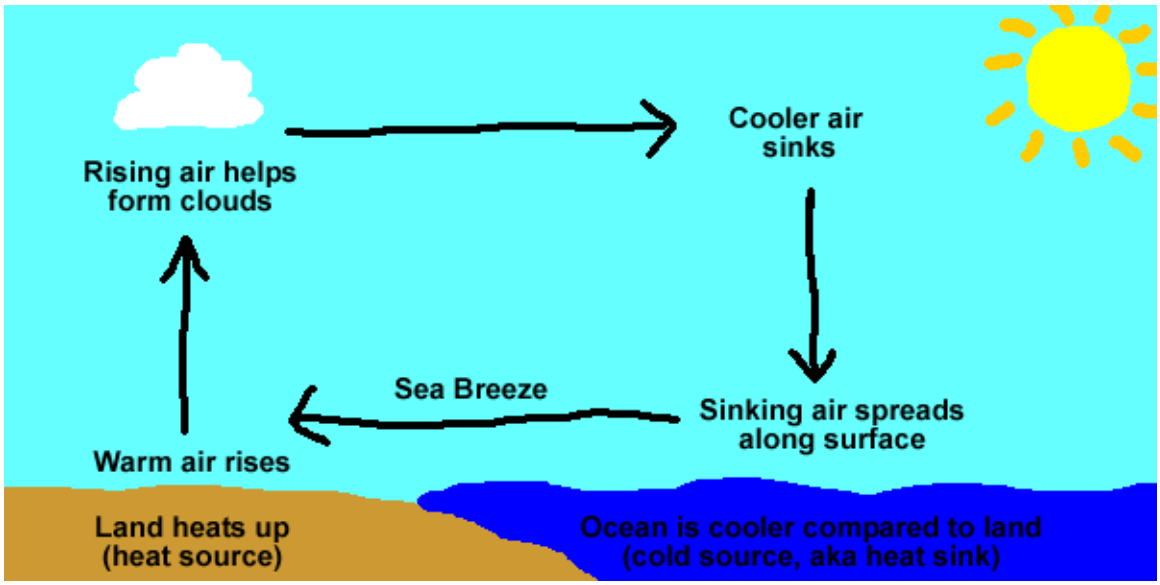

Fig. 1.1. Schematic from the National Weather Service office in Honolulu (http://www.prh.noaa.gov/hnl/kids/activities.php) showing the daytime component of the thermal circulation, with arrows denoting the direction of the flow. The ocean is denoted by dark blue and the land by brown. The arrow on the top of the circulation is part of the return flow that completes the circulation.

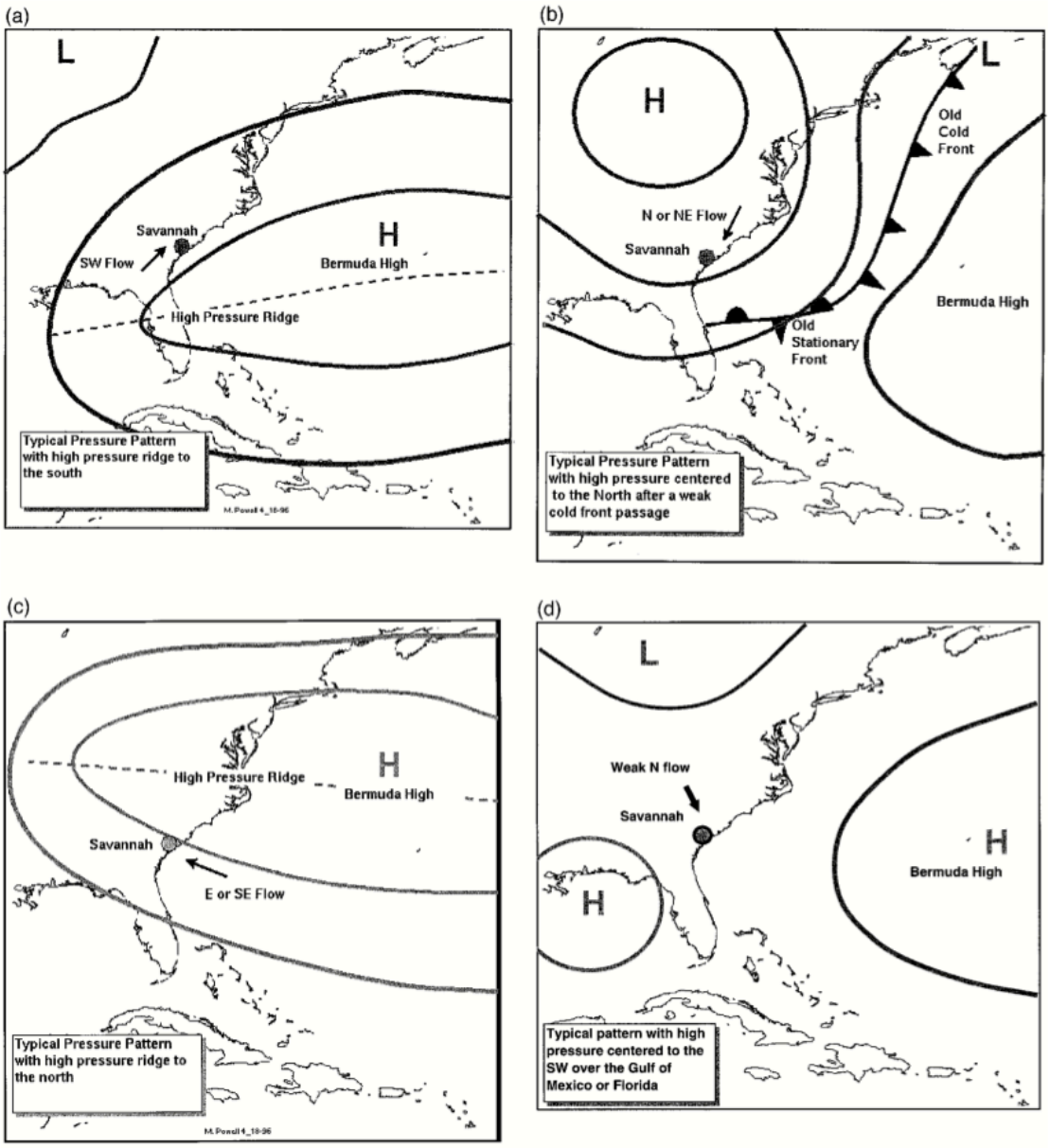

Fig. 1.2. Schematic from Powell and Rinard (1996). Panels show the surface synoptic features and the resultant gradient flow for non-disturbed synoptic days categorized by (a) high pressure ridge to the south, (b) high pressure centered inland to the north or northwest, (c) high pressure ridge to the north, and (d) high pressure centered to the southwest.

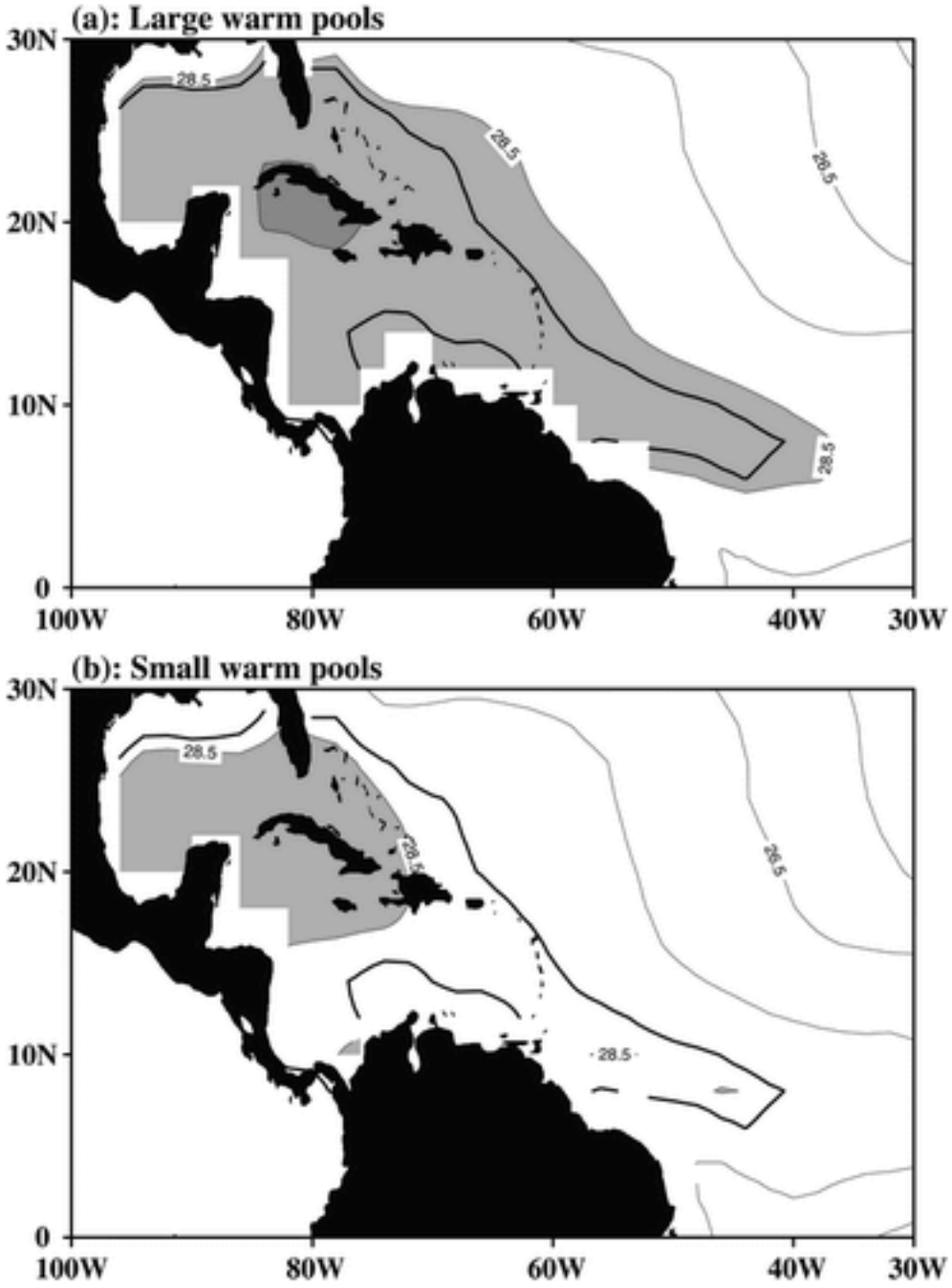

Fig. 1.3. Two schematics showing the AWP. Gray shading denotes the total area of SSTs higher than 28.5°C for (a) large AWP years and (b) small AWP years. The contour lines are isotherms in °C.

CHAPTER TWO

DATA AND METHODOLOGY

2.1 Datasets Used in Study

2.1.1 Model

This study uses the Center for Ocean-Atmospheric Prediction Studies (COAPS) Land Atmosphere Regional Reanalysis over the Southeast United States (CLARReS; Stefanova et al. 2011) to generate the majority of the atmospheric fields discussed in the results. CLARReS consists of the National Center for Environmental Prediction's (NCEP) Experimental Climate Prediction Center (ECPC) Regional Spectral Model (RSM; Juang and Kanamitsu 1994) with lateral boundary forcing from other reanalysis datasets. The RSM is a Fourier-based spectral model; its primitive equations are under the hydrostatic assumption. Table 2.1 shows a list of the parameterization schemes that are used, including the land cover dataset used and topography information. A scale-selective bias corrective scheme (Kanamaru and Kanamitsu 2007) is also applied, which limits the large-scale errors often found in the interior domain of the regional model and allows the down-scaled fields to be less dependent on the domain.

The CLARReS model has two different versions, which are differentiated by the type of reanalysis dataset used as the boundary forcing. The first version that was run was forced by the NCEP Department of Energy (DOE) Reanalysis II (R2; Kanamitsu 2002) dataset; it was dynamically downscaled. The lateral boundary conditions were set during the downscaling process by using wind, temperature, humidity, and surface pressure for every six hours from the R2. This version hereafter will be referenced as CLARReS1.0/R2. The other version is the same as the previous one except that instead of R2, the European Centre for Medium-Range Weather Forecasts (ECMWF) 40 Year Re-analysis (ERA-40; Uppala et al. 2005) was used. This integration of the model will hereafter be referenced as CLARReS1.0/ERA40. Lim et al. (2010) were successful with this downscaling process. In their study, the R2 reanalysis was downscaled to 20 km using the RSM. The precipitation fields from their product were in better agreement with the observations; the root mean square error of the monthly precipitation decreased by over 93% in comparison with the original R2 dataset.

The two model runs are integrated from 1979 to 2001, a 23-year period. The spatial domain of the CLARReS integrations consists of the area between 23.1˚N and 37.5˚N, and between 92.1˚W and 75˚W. This covers almost the entire southeastern United States, the northeastern Gulf of Mexico, and parts of the extreme western Atlantic (Fig. 2.1). However, the domain in most of the figures in this paper is centered on Florida, and therefore most of the model domain is not presented.

The horizontal grid spacing on both model integrations is 10 km, which is considerably smaller than the 2.5˚ (~280 km) horizontal spacing that both the R2 and ERA-40 reanalysis contain. There are 28 sigma levels and 17 pressure vertical levels; the vertical resolution decreases with height. The two-dimensional variables are available hourly whereas the three-dimensional variables are only available every three hours, starting at 7:00 p.m. Therefore, only every three hours will be shown in the examination of the diurnal cycle. However, the two-dimensional fields are examined as well, and the results do not change because of the lower temporal spacing of the three-dimensional variables.

2.1.2 Verification and Other Datasets

Along with the two CLARReS model integrations, numerous other datasets are used to verify that the model results agree with observations. One of these datasets is the extended reconstruction sea surface temperature analysis version 3 (ERSSTv3; Smith et al. 2008), which is provided by the National Oceanic and Atmospheric Administration (NOAA). This SST dataset is also used in the two CLARReS model integrations. Another dataset is the R2 horizontal wind fields, which are monthly averaged and available on a 2.5˚x2.5˚ grid. Both the ERSSTv3 and the R2 analyses have global spatial domains; therefore, they can be used to show the entire AWP.

Two different precipitation observational datasets are used in conjunction with the model to verify the diurnal and interannual variations produced by the CLARReS integrations. The first is the precipitation analysis from the Climate Prediction Center (CPC; Higgins et al. 2000), which consists of station data archives available at one-quarter degree resolutions. The domain for this dataset covers 140˚W to 60˚W and 20˚N to 60˚N, large enough to cover the contiguous 48 states. The smallest temporal spacing that the CPC precipitation can achieve is daily, which would make it unfit for diurnal verification. Therefore, in conjunction with CPC, the NCEP Environmental Modeling Center (EMC) precipitation product (Lin and Mitchell 2005) produced by the National Weather Service (NWS) River Forecast Centers is used for verification. This

product has 4-km grid spacing and is available hourly. However, unlike CPC, the NCEP-EMC gridded precipitation does not consist solely of rain gauge data. Rather, it includes a medley of station data, radar precipitation estimates, and multisensor analysis that includes satellite data. The NCEP-EMC product is available only from 2002 to 2009, which, although it does not overlap with the CLARReS model temporal domain, is sufficient for verifying the climatological diurnal variability of precipitation.

2.2 Methodology

One of the first steps necessary for this study is to establish definitions of large and small AWP. To date, no categorization of the AWP has been accepted by the general scientific community because studies of the phenomenon are relatively recent (since 2001). Wang et al. (2006) have adapted a definition based on their extended reconstructed SST dataset spanning the period from 1950 to 2003. Their study categorized the large (small) AWP years as those in which the AWP size is 25% larger (smaller) than the climatological mean. Using this definition, they found that the large AWPs are almost three times larger than the small AWPs (Fig. 1.3).

The AWP size is calculated for the period 1979–2001 for the ERSSTv3 dataset, and the results are shown in Fig. 2.2. For five of the years, AWP sizes are one standard deviation below the mean (1984, 1986, 1989, 1993, 1994); for four of the years, AWP sizes are one standard deviation above the mean (1981, 1987, 1995, 1998). The remainder of the AWP sizes rest somewhere between $3x10^6$ and $5x10^6$ m^2 with the exception of 1999, which has a slightly higher AWP size and rests very close to the positive standard deviation line. Therefore, 1999 is added to the large AWP composite, and thus each composite comprises five years. Table 2.2 shows the rankings of all the years.

Next, composites are made of SST and 850-hPa winds using this study's definition of large/small AWP, shown in Fig. 2.3. These composites have been computed using the summer months only (hereafter JJA) since the focus of this paper is the sea breeze variations in Florida, which are most significant during JJA. Both the large and the small AWP composites are similar to the schematic provided by Wang et al. (2006; Fig. 1.3). Notice that even though most of the AWP is located in the Gulf of Mexico and the Caribbean Sea, the greatest changes take place in the Atlantic Ocean. Even so, the SSTs are generally higher in the AWP for large AWP years. In conjunction with the SSTs, the 850-hPa winds also agree with the findings in Wang et al. (2006). The difference plot (Fig. 2.3c) shows that in both the Gulf of Mexico and the Caribbean Sea, the

large-scale flow at 850 hPa is weaker for large AWP years. This is supported in the literature that describes a weakening of the Great Plains low-level jet (GPLLJ) for the large AWP case (Wang et al. 2006; Wang et al. 2008).

Climatology JJA precipitation composites are also created using the CPC observations (Fig. 2.4). The most striking difference between the large and small AWP years is the negative precipitation anomaly that exists in the Florida panhandle, especially west of 84°W. Although this does not prove that modulation of Florida convection by the AWP exists, it does suggest the potential for low-frequency variations of the sea breeze to be present because of the AWP phenomenon. Although peninsular Florida, especially the interior, also shows a negative anomaly, the signal is weaker than for the panhandle, and thus less emphasis is placed on this region. Therefore, cross sections appearing later will highlight the panhandle region between 84°W and 88°W to hone in on the area that contains the strongest low-frequency signal.

In the next section these low-frequency variations are explored, a modulation is shown to exist, and the reason for the sea breeze variability for the Florida panhandle during JJA is diagnosed. This is accomplished by using a variety of spatial maps and cross sections. The cross sections are located along the latitude of 30.5°N since the emphasis will be on the Florida panhandle region (Fig. 2.5). This latitude is chosen to sample as much of the panhandle as possible and avoid the ocean as much as possible.

Table 1: A brief outline of the Regional Spectral Model.

Model Feature	**Description**
Resolution	10-km horizontal resolution, 28 vertical terrain-following sigma levels
Domain	~ 23^0S to 37.5^0 N and 98^0W to 75^0W
Topography	30-min USGS topography
Vegetation map	USGS converted to 12 NOAH vegetation types (Loveland et al. 1995)
Land surface scheme	NOAH with 4 soil levels (Ek et al. 2003)
PBL scheme	Non-local; Hong and Pan (1996)
Radiation Scheme	Chou and Lee (1996); Chou and Suarez (1994)
Cloud water scheme	Diagnosed from relative humidity; Slingo (1987)
Convection scheme	Simplified Arakawa Schubert Scheme; Pan and Wu (1994)

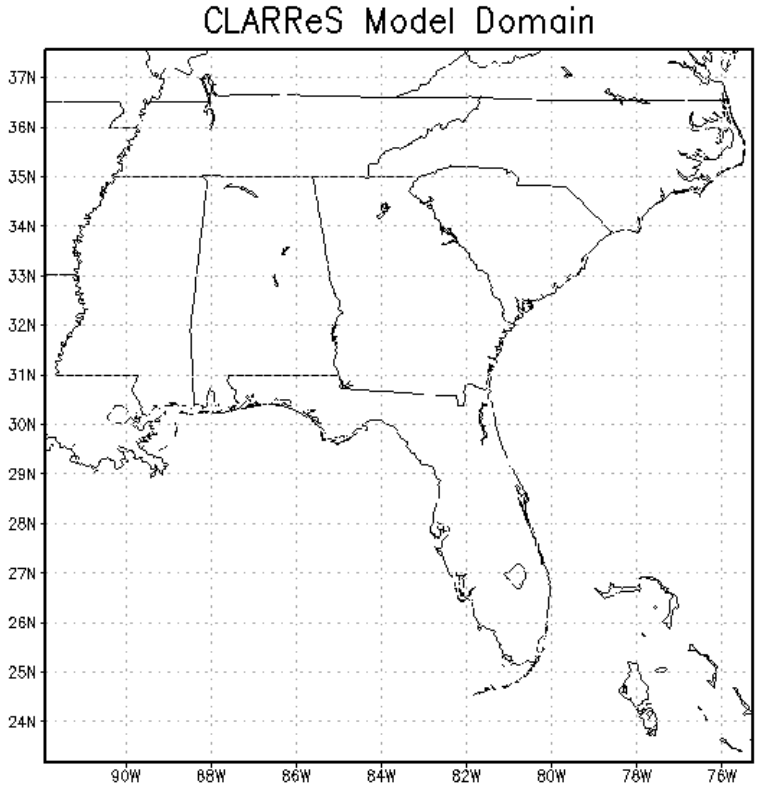

Fig. 2.1. The entire spatial domain of both the CLARReS1.0/R2 and CLARReS1.0/ERA40 model integrations.

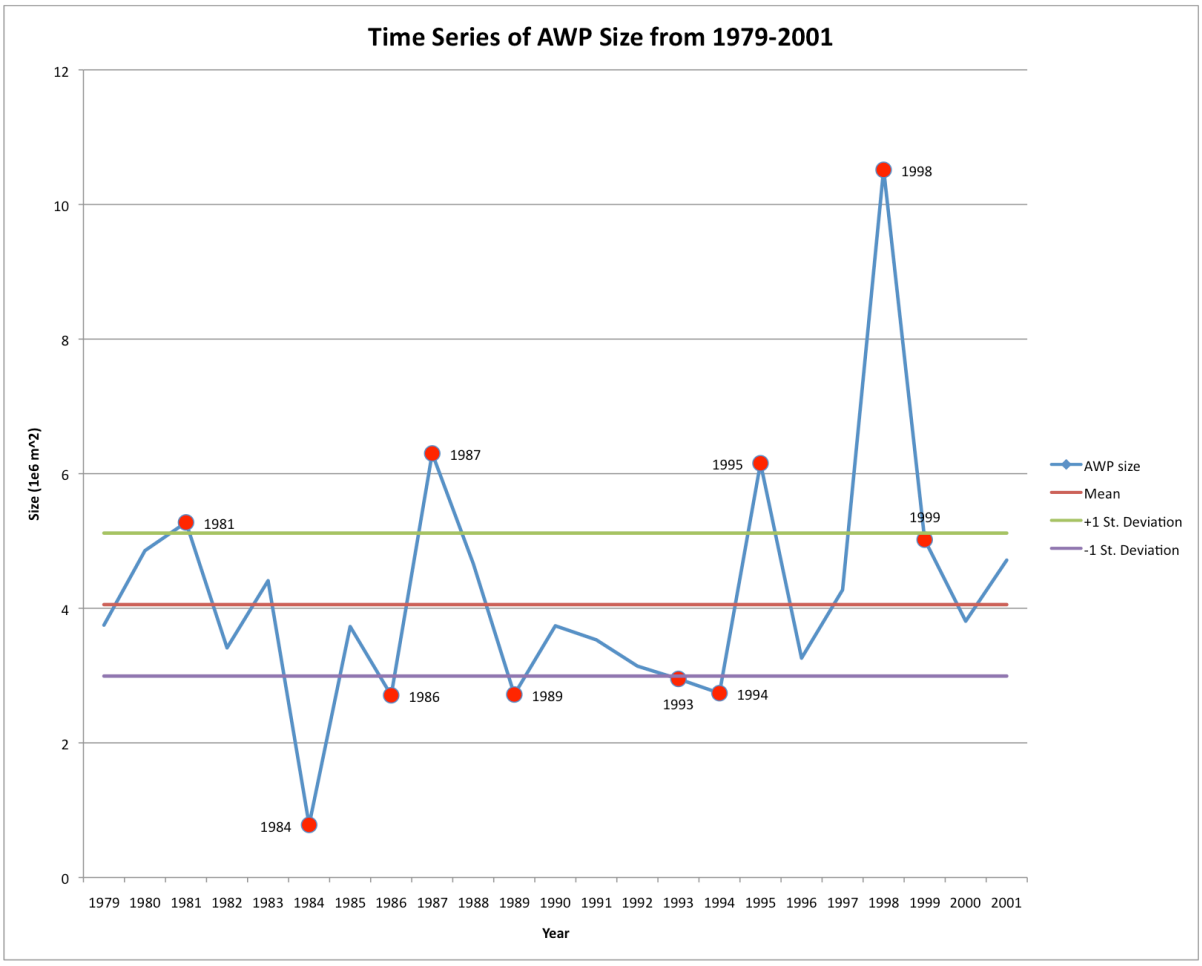

Fig. 2.2. Time series of AWP size represented by the blue contour. The year is on the x-axis, and the size (multiplied by $1x10^6$) is on the y-axis. The units are m^2. The mean and the first standard deviations are shown (see legend to the right). The five top and five bottom sizes are denoted by red dots.

Table 2: The year and the size of the AWP for that year. The years chosen to be large AWP years are in red, and the years chosen to be small AWP years are in blue.

Year	Size (km)	Year	Size (km)
1) 1998	1.05×10^7	13) 1990	3.74×10^6
2) 1987	6.30×10^6	14) 1985	3.73×10^6
3) 1995	6.15×10^6	15) 1991	3.53×10^6
4) 1981	5.28×10^6	16) 1982	3.41×10^6
5) 1999	5.02×10^6	17) 1996	3.26×10^6
6) 1980	4.86×10^6	18) 1992	3.14×10^6
7) 2001	4.72×10^6	19) 1993	2.95×10^6
8) 1988	4.66×10^6	20) 1994	2.74×10^6
9) 1983	4.41×10^6	21) 1989	2.72×10^6
10) 1997	4.27×10^6	22) 1986	2.71×10^6
11) 2000	3.81×10^6	23) 1984	7.82×10^5
12) 1979	3.75×10^6		

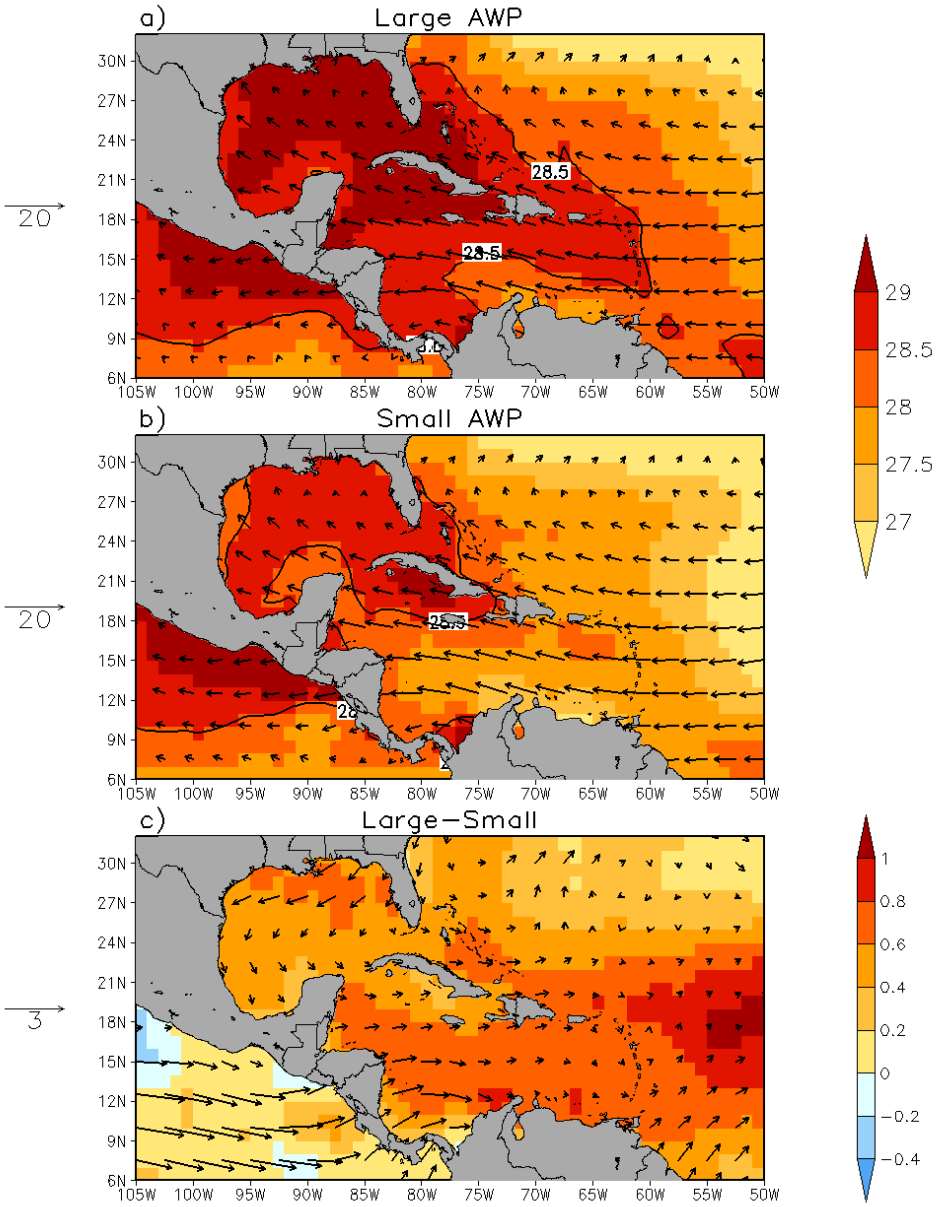

Fig. 2.3. The shading shows the SST in units of ^{0}C from the ERSSTv3 observational dataset, and the vectors are 850-hPa winds taken from the NCEP-DOE R2 dataset (in units of ms^{-1}). The panels are (a) the large AWP summer (JJA) composite mean, (b) the small AWP JJA composite mean, and (c) the difference (large-small) between the two composite means. The scale vector is given by the arrow on the left of the panels.

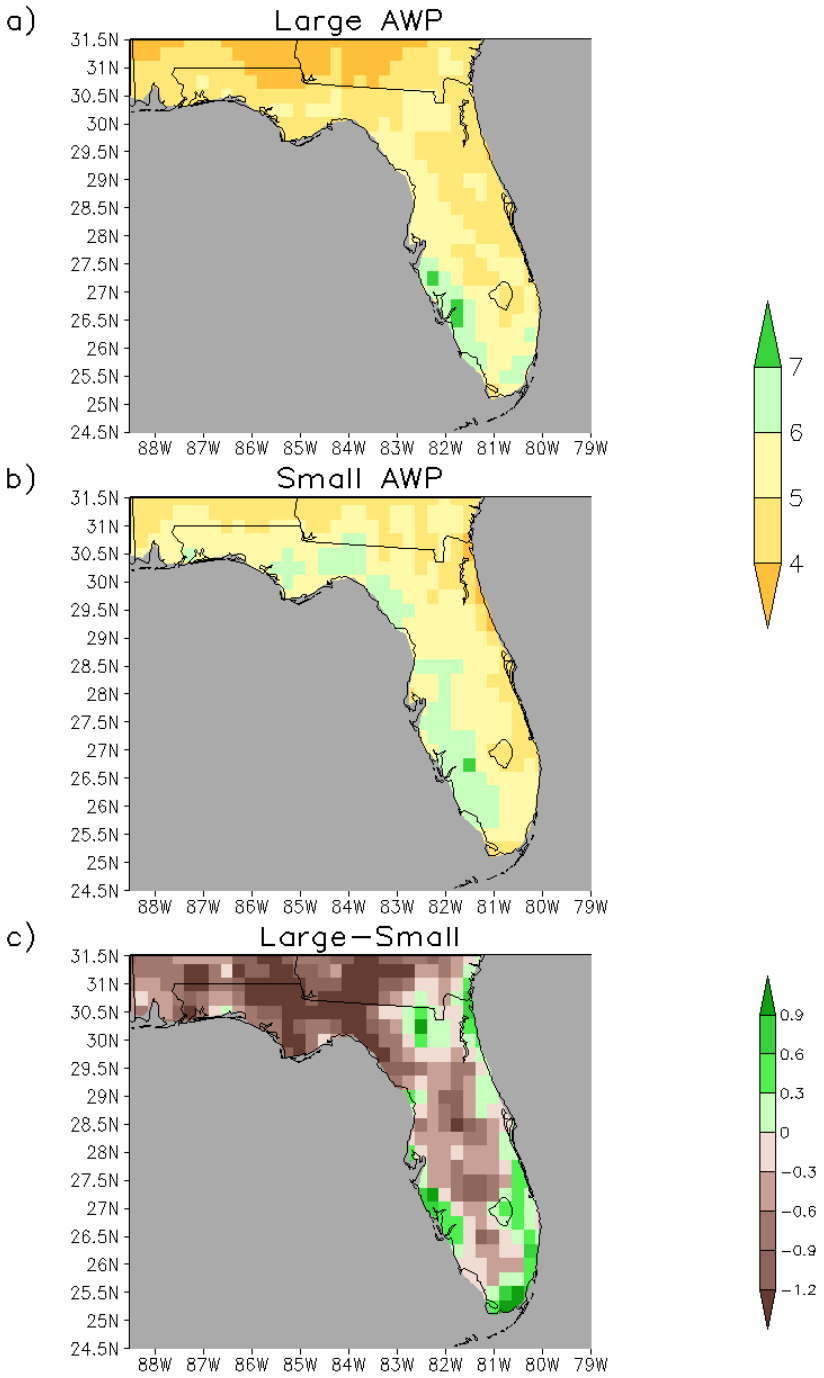

Fig. 2.4. Precipitation in units of mm day^{-1} for (a) the large AWP JJA composite mean, (b) the small AWP JJA composite mean, and (c) the difference (large-small) between the two composite means.

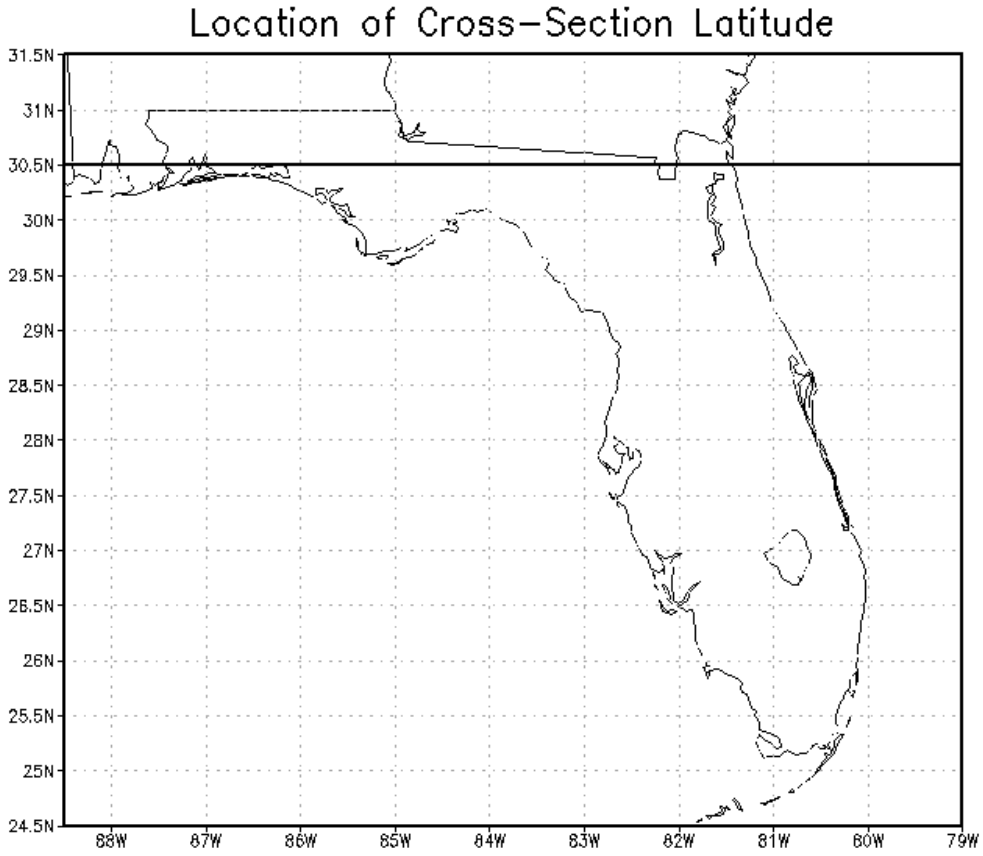

Fig. 2.5. The 30.5°N latitude and the spatial domain for the majority of the area plots.

CHAPTER THREE

RESULTS

3.1 Climatology of the Diurnal Variability over Florida

First, this study addresses the diurnal nature of the sea breeze and verifies the model's ability to simulate diurnal changes in the sea breeze and associated convection. This objective is accomplished by first using the observations taken from the NCEP-EMC gridded precipitation estimates (Fig. 3.1) to examine the climatological mean diurnal convection cycle. Figure 3.1 indicates that daily convection reaches a minimum at 4:00 a.m., and then a gradual increase in the precipitation occurs throughout the morning hours. Significant convection, most notably in southern Florida, arises at 1:00 p.m. The diurnal maximum of precipitation for the entirety of Florida occurs at 4:00 p.m., and after the maximum a gradual decrease of precipitation occurs into the overnight hours.

Figures 3.2 and 3.3 show the climatological mean diurnal precipitation cycle for CLARReS1.0/R2 and CLARReS1.0/ERA40, respectively. The smooth appearance of the contours in the models in comparison to the NCEP-EMC product is caused by the lower grid spacing of the CLARReS model integrations. The products of both the CLARReS1.0/R2 and the CLARReS1.0/ERA40 underestimate the precipitation in comparison to the NCEP-EMC product, but the CLARReS1.0/ERA40 is closer in magnitude to the observations, particularly over southern Florida. More importantly, both model integrations capture the timing and nature of the diurnal cycle. The CLARReS1.0/R2 and CLARReS1.0/ERA40 indicate precipitation minimums occurring at 4:00 a.m. and precipitation maximums at 4:00 p.m. The growth and demise of the diurnal peak is also simulated well in both model integrations. The correct reproduction of the climatological average precipitation diurnal cycle was a primary motivation for using the RSM downscaled models.

In addition to the precipitation, the climatological mean diurnal variation of the planetary boundary layer (PBL) height and the meridional plus vertical winds are plotted. These variables are averaged over a line of latitude (30.5°N; see Fig. 2.5 for a location reminder) using CLARReS1.0/R2 (Fig. 3.4) and CLARReS1.0/ERA40 (Fig. 3.5). Although the vectors point left

and right, that is not a reference to west-east zonal movement. Rather, vectors pointing toward the right hint at northerly flow and vectors pointing to the left indicate southerly flow. Using this reasoning, one can see that winds are generally from the south in the low levels over the panhandle; increased wind direction variability exists in the midlevels. However, because the meridional wind component is used, the thermal circulation is misrepresented east of 84°W. At this location the thermal circulation is perpendicular to the coast, and the thermal circulation is parallel to a zonal flow. Another important note is that the vectors represent both the large- and small-scale flows. The idea of separating the large- and small-scale flows was considered, but the separation was too difficult to do correctly.

Figure 3.4 shows that during the overnight hours the CLARReS1.0/R2 model designates a primarily meridional flow over the Florida panhandle. Areas of slight vertical motion might correspond to the land breeze aspect of the diurnal thermal circulation (Biggs and Graves 1962); the signal is not as strong as it is during the day. The PBL is also quite shallow over land overnight, with increases occurring at 10:00 a.m., corresponding to the start of diurnal heating. The PBL reaches a maximum at 1:00 p.m., and at that time the vertical velocities also increase. Upward vertical velocities exist over the land areas, and downward vertical velocities exist over water. The vertical velocity anomalies are a direct result of the model simulating the effects of the thermal circulation, a daily occurrence during JJA in Florida. The thermal circulation is noisier over the western part of the cross section, a direct result of numerous bays and other small water bodies in the area (Fig. 2.5). These vertical velocities reach a peak at 4:00 p.m. while the PBL height starts to decrease. Since the precipitation maximum is also at 4:00 p.m. the CLARReS1.0/R2 depicts this PBL decrease because the updrafts from the convection in the area have broken through the PBL and consequently mix it out. The thermal circulation is nonexistent by 7:00 p.m. and the PBL decreases to less than 500 meters as the night progresses. The flow switches back to large-scale meridional flow. The CLARReS1.0/ERA40 also demonstrates this diurnal picture, with the main difference being it is more persistent with the small-scale perturbations at 7:00 p.m.

3.2 Climatology of the Interannual Variability over Florida

Next, the interannual variability of the precipitation is examined. Figure 3.6 contains the AWP composites of precipitation and their differences from the CLARReS1.0/R2; the model's simulation of the interannual variability is evaluated by comparing it with the observations in

Fig. 2.4. Looking at the large and small AWP composites, one notices that the CLARReS1.0/R2 does not do well in depicting these composites. For the panhandle of Florida, CLARReS1.0/R2 overestimates the amount of precipitation for both composites. The locations of the precipitation maximums and minimums are not collocated either, although the model does appear to reproduce the precipitation maximums along the Gulf coast of Florida for small AWP years. What the model does simulate well is the strong negative anomaly along the panhandle of Florida west of 84˚W. However, the interannual signal along peninsular Florida is not captured very well in CLARReS1.0/R2, in particular across the region between Jacksonville and Tampa. There are several possible reasons for the model's inability to capture the interannual signal. One is the more complicated nature of the sea breeze interactions in this part of the state caused by interactions of two sea breezes emanating from the coasts. Another is that the peninsula of Florida experiences more tropical storms than its panhandle counterpart, which introduces a component unrelated to the diurnal precipitation and thermal circulation.

The CLARReS1.0/ERA40 (Fig. 3.7) does worse than the CLARReS1.0/R2 (Fig. 3.6) in simulating the precipitation and shows gross estimation in both composites. This model integration is persistent in showing high precipitation maximums in south Florida, unlike CLARReS1.0/R2 and the observations. Again, because of the inherently more complicated nature of the sea breeze in peninsular Florida, the model integrations have more trouble simulating the interannual variability of the precipitation in this region. In the composite difference the CLARReS1.0/ERA40 is similar to CLARReS1.0/R2 except that the positive precipitation anomalies are more pronounced over central Florida, and the negative anomalies are farther west (86˚W-88˚W) in the panhandle.

Both model integrations do poorly with depicting the interannual variability of the precipitation, yet some agreement exists on the negative anomaly for large AWP years over the panhandle of Florida. The rest of the chapter will focus on explaining the low-frequency variations of the sea breeze and related convection over the Florida panhandle, primarily west of 84˚W. Owing to the more complicated nature of the mesoscale and synoptic systems in peninsular Florida, the low-frequency variations of the sea breeze in that region are not distinguishable.

3.3 Diagnostic Analysis of the Low-frequency Variations over Panhandle Florida

The first step in identifying the mechanism behind the interannual variability is to examine the temperature gradient between the land and sea because the differential heating between the land and sea instigates the sea breeze. Both the CLARReS1.0/R2 (Fig. 3.8) and CLARReS1.0/ERA40 (Fig. 3.9) are in good agreement with the composite mean temperatures. They show that for large AWP years the land temperatures are slightly warmer than they are for small AWP years. Ocean temperatures are quite stagnant when compared to the diurnal heating changes that occur over land and do not change significantly day to day. Therefore, the increased heating over land for large AWP years by both model integrations hints that the temperature gradient between land and ocean is higher for large AWP years. A larger temperature gradient increases the strength of the thermal circulations, enhances the sea breeze, and thus leads to more convection. For this reason, a contradiction exists during large AWP years in that a larger temperature gradient is present but less convection falls over the Florida panhandle.

Next, the diurnal change of the composite differences of precipitation is examined. The CLARReS1.0/R2's precipitation is shown in Fig. 3.10, and the CLARReS1.0/ERA40's precipitation is shown in Fig. 3.11. The CLARReS1.0/R2 shows the negative anomalies in the Florida panhandle are the strongest at 4:00 p.m., and the precipitation pattern at 4:00 p.m. matches the seasonal composite difference (Fig. 3.6c). This match suggests that the sea breeze and precipitation are modulated by the interannual variations of the AWP. Figure 3.11 does not show the negative precipitation anomaly over the panhandle of Florida, but because of the westward displacement (Fig. 3.7c) of the negative anomaly, it is more difficult to complete this analysis for the CLARReS1.0/ERA40 integration. However, the precipitation patterns at 1:00 p.m. and 4:00 p.m. match the seasonal composite mean difference (Fig. 3.7c) quite well, and negative anomalies are present west of 86˚W. Even though the signal is not as strong as that in the CLARReS1.0/R2, the CLARReS1.0/ERA40 hints that the sea breeze and convection are modulated by the AWP variations.

At this point, albeit the modulation of the sea breeze seems apparent, the evidence provided to explain the low-frequency variations in the sea breeze convection is contradictory. Therefore the large-scale effects on the interannual variability are examined. The idea that the large-scale flow influences the sea breeze is well supported in the literature (see Chapter 1). Therefore the cross section of the PBL and meridional and vertical winds is revisited; however,

this time the composite mean difference at 4:00 p.m. is plotted for CLARReS1.0/R2 (Fig. 3.12) and CLARReS1.0/ERA40 (Fig. 3.13). The increased PBL for large AWP years fits for two different reasons: if there is less or weaker convection, the updrafts will not push through the inversion and disrupt the PBL as much, and if the land temperatures are warmer, this will help sustain the dry adiabatic lapse rates below the PBL, increasing its height. The thermal circulations are also apparent at this time for both the large and small AWP years, and they seem to be more pronounced for the large AWP years (Figs. 3.12a, 3.13a). However, recall that both the large- and small-scale flows are represented on these plots, and what becomes evident in Figs. 3.12c and 3.13c is that anomalous large-scale subsidence takes place in large AWP years (although it is displaced westward in the CLARReS1.0/ERA40).

One explanation of this large-scale subsidence anomaly is that it is related to the North Atlantic subtropical high (NASH, Fig. 3.14). Preliminary work by Li et al. (2011) showed that large-scale subsidence over the southeast is related to the NASH. Wang et al. (2006) also described NASH changes that were related to the variability of the AWP. Figures 3.15 and 3.16 show the composite mean and difference of mean sea level pressure and 850-mb winds from CLARReS1.0/R2 and CLARReS1.0/ERA40, respectively. Both model integrations show that during large AWP years, the NASH weakens and displaces farther eastward. The NASH variations, in turn, introduce an anomalous meridional flow over the southeast United States and the Florida panhandle (Figs. 3.15c, 3.16c). Thus, a collocation of anomalous meridional flow and large-scale subsidence exists over the Florida panhandle. These components are related as shown by the principles of Sverdrup vorticity balance (Rodwell and Hoskins 2001).

Hoskins (1996) described the interactions between the monsoon heating and the persistence of subtropical anticyclones using the Sverdrup vorticity balance (Fig. 3.17). As the summer begins, the monsoon heating moves poleward on land. The movement of the monsoon forces the descent to intensify westward and poleward of the monsoon heating over the ocean. A positive feedback loop is generated where the descent causes enhanced diabatic cooling, and that cooling enhances the descent. Then, to be consistent with the vorticity balance, anomalous equatorward flow occurs over regions of maximum descent. Thus, the Sverdrup vorticity balance describes a relationship between the meridional flow and vertical motions (Rodwell and Hoskins 2001, Zhou et al. 2009).

This study shows the derivation the Sverdrup vorticity balance starting with the absolute vorticity equation,

$$\frac{d(\zeta + f)}{dt} = -(\zeta + f)(Divergence) + Twisting + Solenoidal \quad (1)$$

in which ζ is the relative vorticity, and f is the Coriolis parameter. To obtain Sverdrup vorticity balance, assumptions are applied to the above equation. The first assumption is that for large-scale flow the last two terms can be neglected. Applying this assumption and expanding the total derivative in (1) leaves

$$\frac{\partial(\zeta + f)}{\partial t} + u\frac{\partial(\zeta + f)}{\partial x} + v\frac{\partial(\zeta + f)}{\partial y} = -(\zeta + f)(Divergence) \quad (2)$$

In the subtropics, the Coriolis term is much greater than the relative vorticity when applied to a scale analysis, so the relative vorticity can be neglected.

$$\frac{\partial f}{\partial t} + u\frac{\partial f}{\partial x} + v\frac{\partial f}{\partial y} = -fD \quad (3)$$

The second term on the left-hand side can be canceled because the Coriolis force does not vary along latitude. The last assumption that is applied is to assume a steady state. This assumption is reasonable since the NASH is a permanent feature that does not vary daily.

$$v\frac{\partial f}{\partial y} = -fD \quad (4)$$

Equation (4) describes the Sverdrup vorticity balance. If one applies the continuity equation, then the Sverdrup relation takes a form that is most common in the literature.

$$\frac{\partial f}{\partial y} = \beta \quad , \quad \frac{\partial u}{\partial x} + \frac{\partial v}{\partial y} = Divergence = -\frac{\partial \omega}{\partial p}$$

$$\beta v = f\frac{\partial \omega}{\partial p} \quad (5)$$

Whether one uses (4) or (5), the equation makes it easy to see how the relationship works. When there is anomalous poleward flow, rising motion exists; for equatorward flow, sinking motion exists.

To examine the left-side term the meridional flow from both model integrations (Figs. 3.18, 3.19) are plotted along the 30.5°N latitude. The composite differences show that there is anomalous equatorward flow in large AWP years from both the CLARReS1.0/R2 and the CLARReS1.0/ERA40. Then, to complete the investigation of the equation, omega from both

model integrations is represented in Fig. 3.20 (CLARReS1.0/R2) and Fig. 3.21 (CLARReS1.0/ERA40). Positive omega values in regions west of 84˚W in Fig. 3.20 show that there is large-scale subsidence. The CLARReS1.0/ERA40 simulates the same process, although it displaces the subsidence westward by two longitudes. This displacement is to be expected given the location of the subsidence and precipitation anomalies previously noted (Figs. 3.13, 3.7). Therefore, both of the model integrations correctly display the Sverdrup vorticity balance as the mechanism that links the large-scale flow pattern to areas of descent. The main driver of this mechanism is the position and intensity changes of the NASH.

However, even though the suppression of the convection over the Florida panhandle for large AWP years is explained, the issue of the stronger circulations for large AWP years is not yet resolved. To further explore this matter, the moisture balance equation is used, which is

$$\underset{Term1}{\frac{\partial Q}{\partial t}} = \underset{Term2}{-\nabla \bullet M} + \underset{Term3}{E} - \underset{Term4}{P} \qquad (6)$$

where

$$-Q = \frac{1}{g}\int_{P_s}^{10mb} qdp \quad \text{and} \quad M = \frac{1}{g}\int_{P_s}^{10mb} \vec{V}qdp$$

In equation (6), term 1 is the precipitable water tendency term, term 2 is the moisture flux convergence term (where positive values indicate convergence), term 3 is evaporation, and term 4 is precipitation. For both model integrations, the terms of the moisture budget equation are plotted (Figs. 3.22, 3.23) for 4:00 p.m., where the precipitable water tendency term is calculated as a residual. Both the CLARReS1.0/R2 and the CLARReS1.0/ERA40 are in good agreement over the terms in the moisture budget.

In the composite differences, there is anomalous convergence of moisture flux over the panhandle of Florida, especially in regions west of 84˚W. The reasons for this anomaly were not investigated, but it is possible that the anomaly is due to stronger circulations occurring during large AWP years (Figs. 3.12, 3.13). The precipitation fields were discussed at length earlier (Figs. 3.10 and 3.11). Both models illustrate that evaporation is not significant in the interannual variability and thus can be discarded. The precipitable water tendency residuals should be strongly positive, as Figs. 3.22d and 3.23d indicate. Therefore, the precipitable water in the atmospheric column should be anomalously positive for large AWP years. This anomalous

precipitable water is shown in Figs. 3.24 and 3.25. The composite difference in both model integrations shows that the precipitable water content is higher at 4:00 p.m. for large AWP years.

An understanding of interannual sea breeze variability is obtained by using the moisture budget equation and Sverdrup vorticity balance together. Over the course of a day, there is increased moisture flux convergence over the panhandle of Florida for large AWP years. The increased moisture flux convergence could be because of stronger land-ocean temperature gradients, or because of other factors. The thermal circulation is stronger as well. However, though these phenomena occur, large-scale subsidence exists because the NASH weakens and moves eastward during large AWP years. Therefore, the convection is suppressed, and instead of water precipitating out of the column, the column accumulates increasing amounts of moisture, as the moisture budget equation indicates. In small AWP years, the suppression is less, the convection is more frequent, and thus more moisture is allowed to leave the atmospheric column.

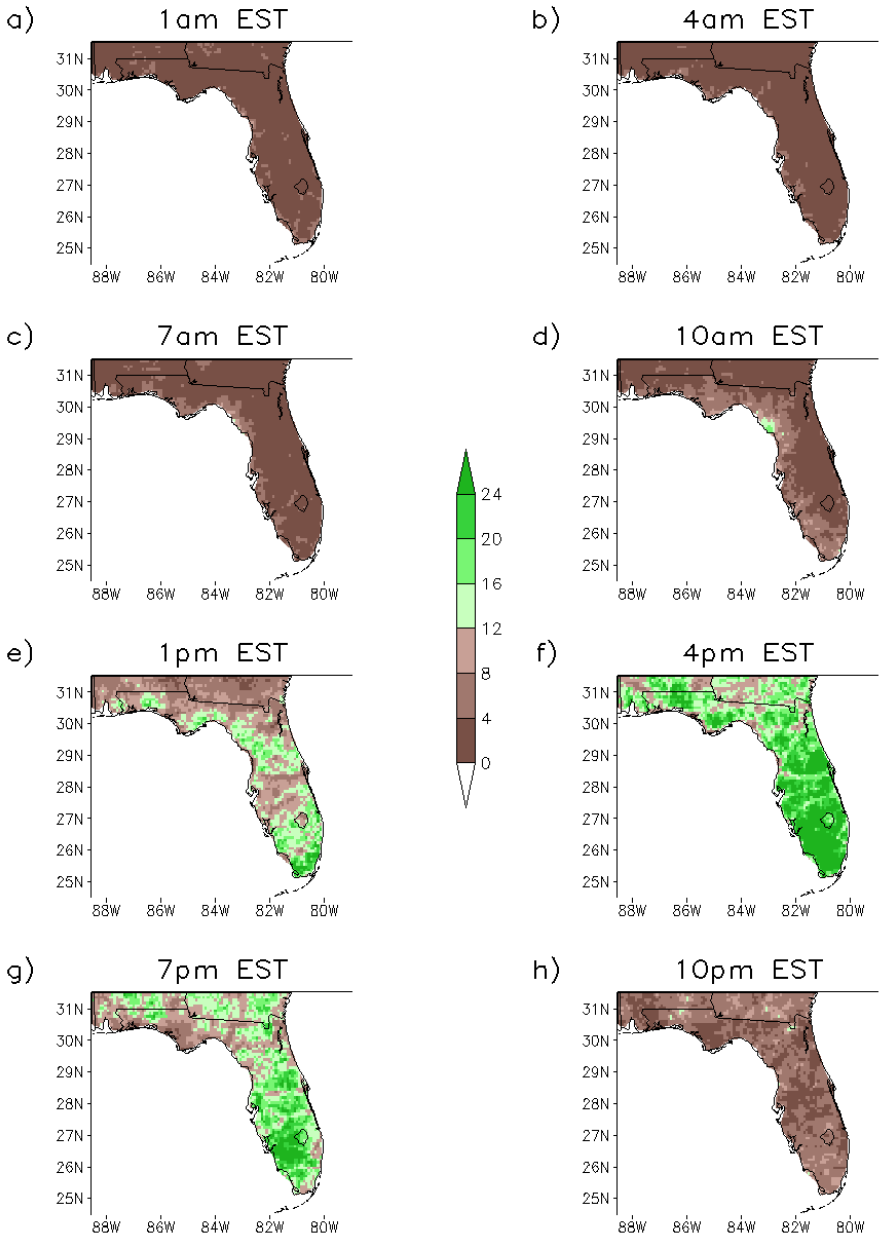

Fig. 3.1. Plot containing precipitation averaged at one time (denoted by the panel titles) over JJA for the entire temporal domain (1979-2001). The units are in mm day^{-1}. Precipitation data are from the NCEP-EMC dataset.

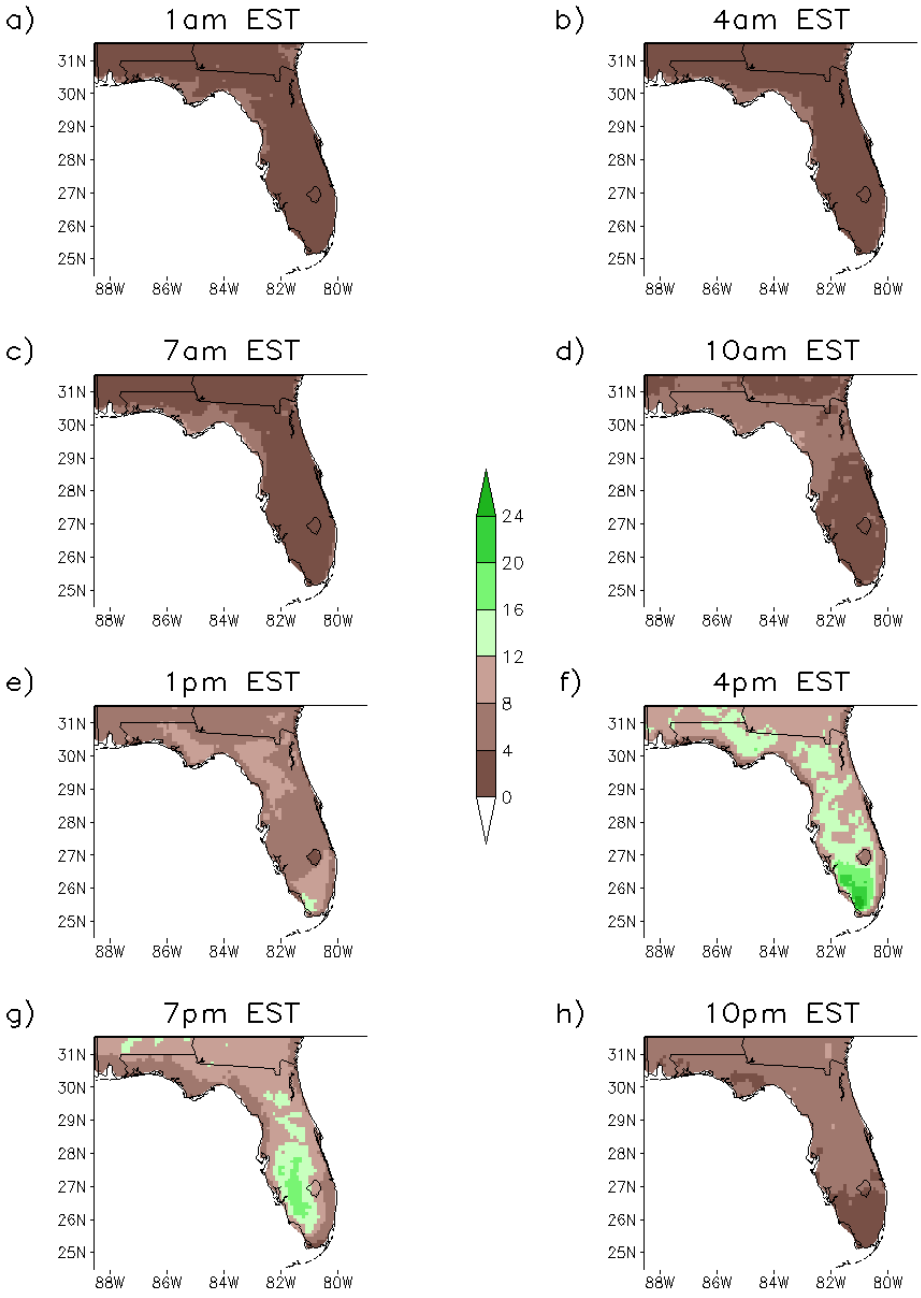

Fig. 3.2. Same as Fig. 3.1 except the data are from the CLARReS1.0/R2 model run.

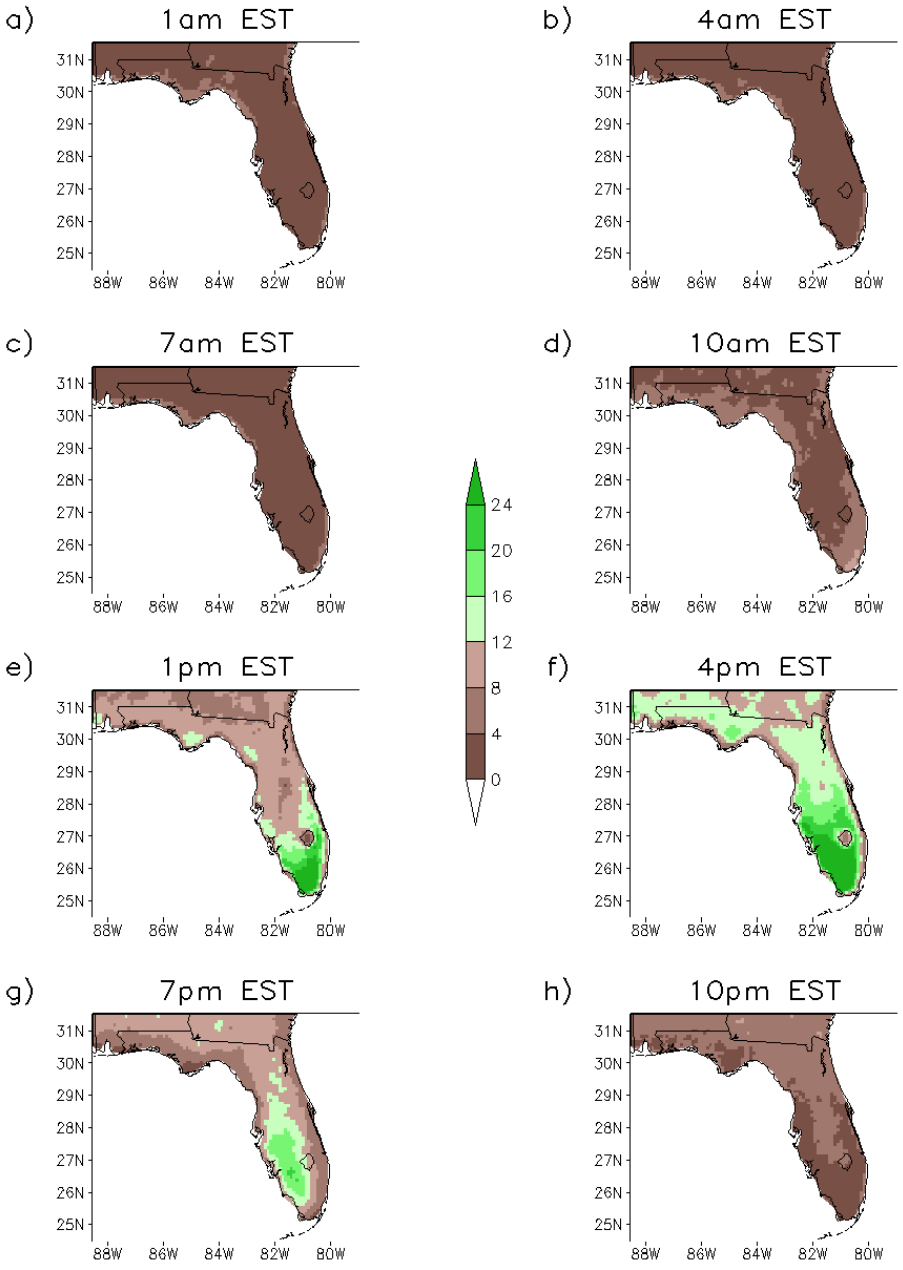

Fig. 3.3. Same as Fig. 3.1 except the data are from the CLARReS1.0/ERA40 model run.

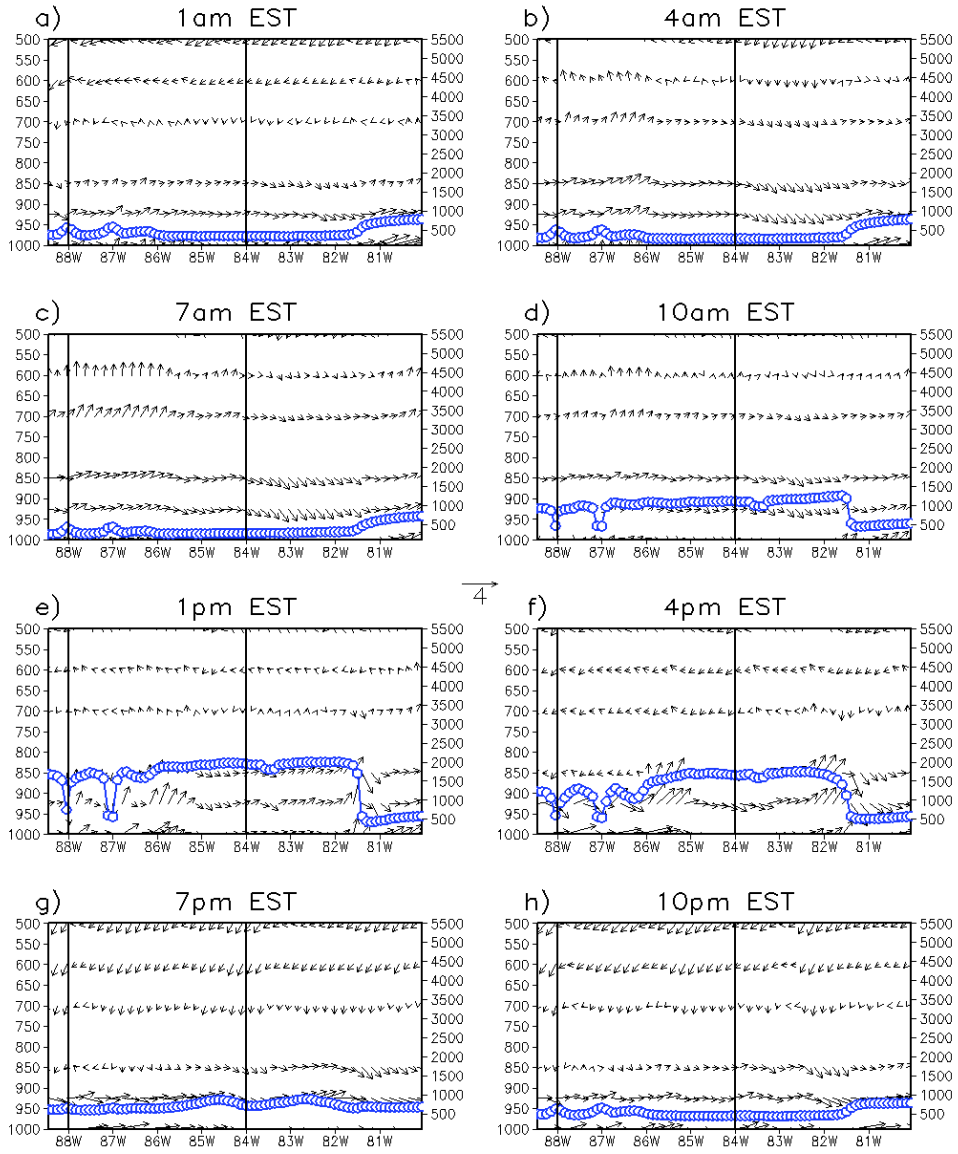

Fig. 3.4. Cross sections through 30.5°N. The vectors indicate the meridional and vertical wind components from the CLARReS1.0/R2 model integration averaged at one time (denoted by the panel titles) over JJA from 1979 to 2001 in units of ms^{-1}. The vertical velocities are scaled by 100, and the arrow in the middle gives the scale vector. The left y-axis denotes the height in millibars as a reference to the wind. The blue contour is the planetary boundary layer height in meters from the CLARReS1.0/R2 model integration, averaged the same way as the winds, which are along the right y-axis. The black perpendicular lines mark the locations of 84°W and 88°W.

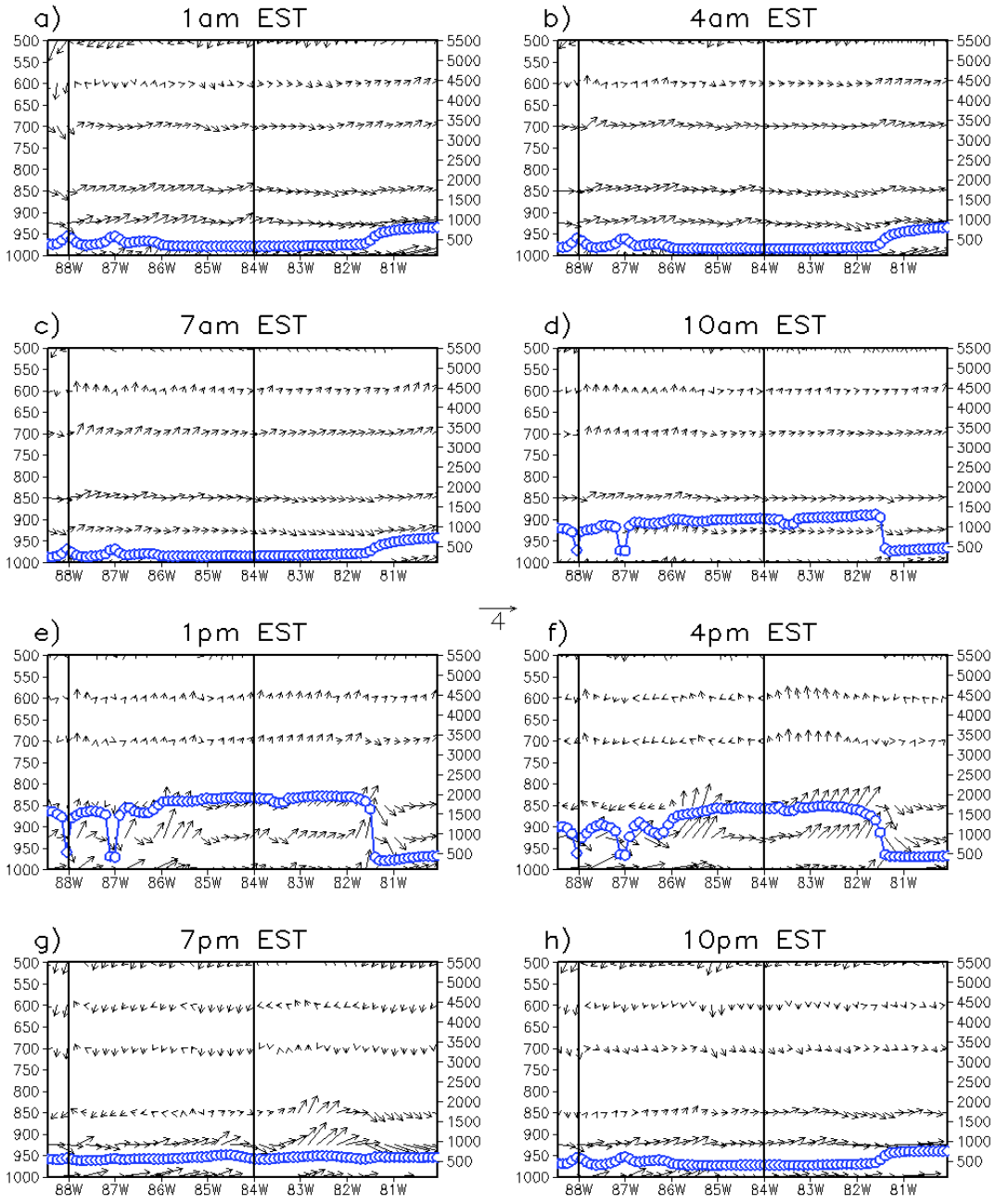

Fig. 3.5. Same as Fig. 3.4 except the variables are from the CLARReS1.0/ERA40 model run.

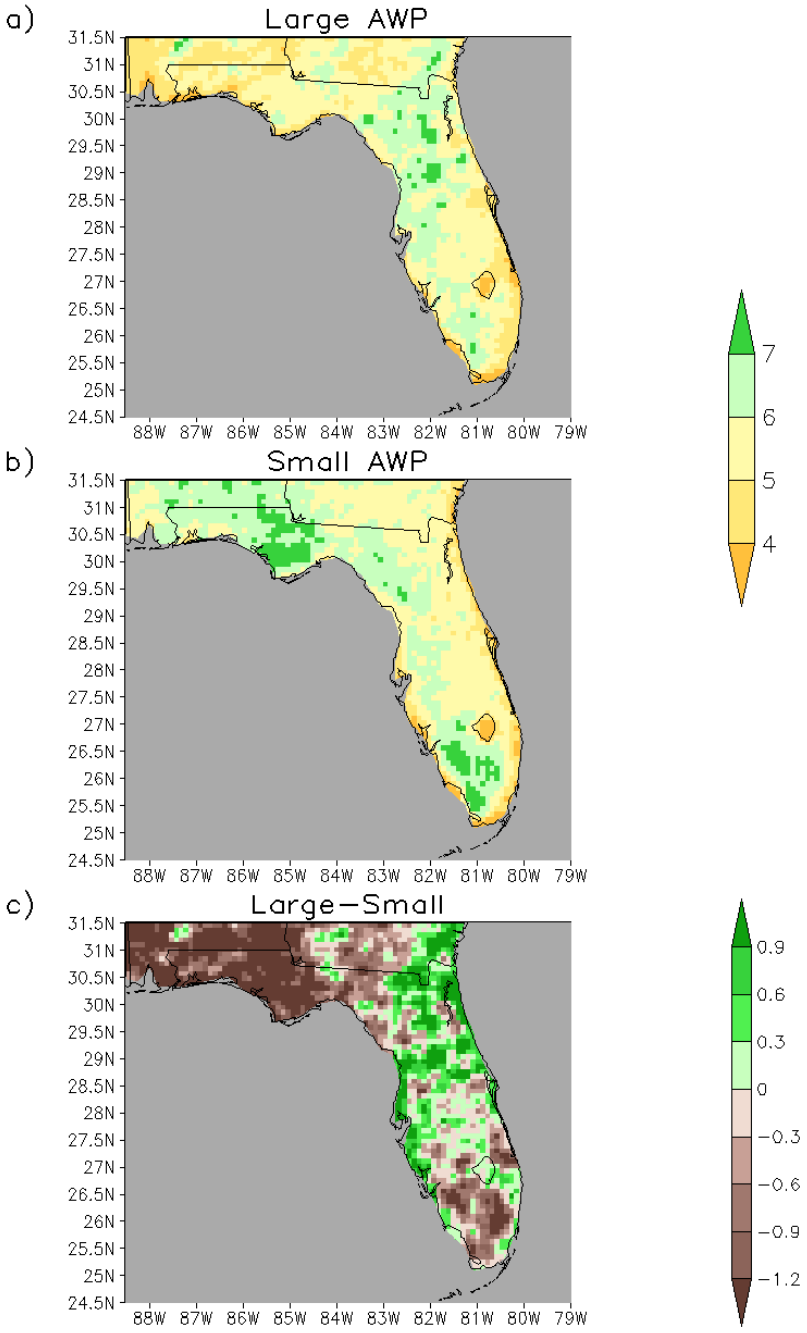

Fig. 3.6. Same as Fig. 2.4 except the data are from the CLARReS1.0/R2 model run.

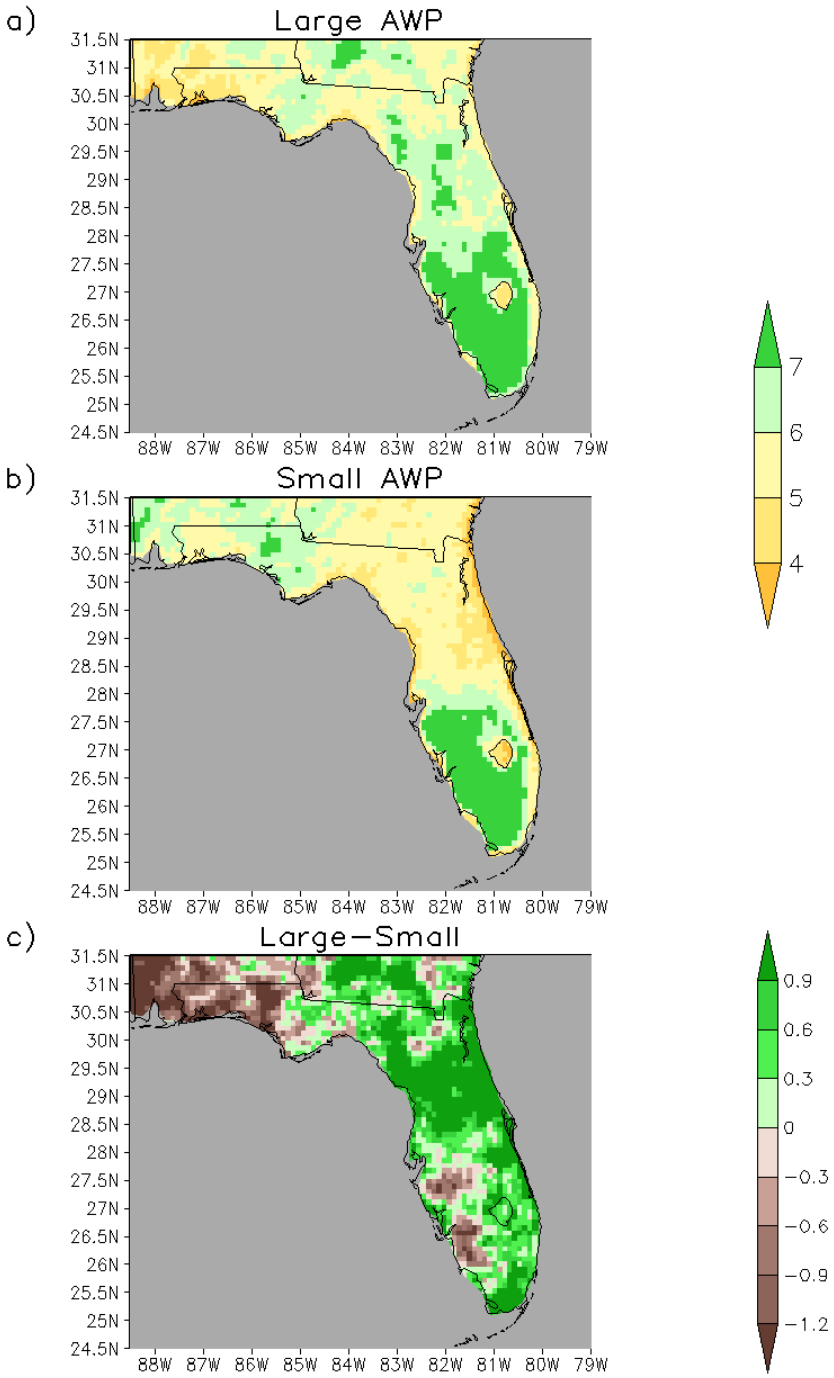

Fig. 3.7. Same as Fig. 2.4 except the data are from the CLARReS1.0/ERA40 model run.

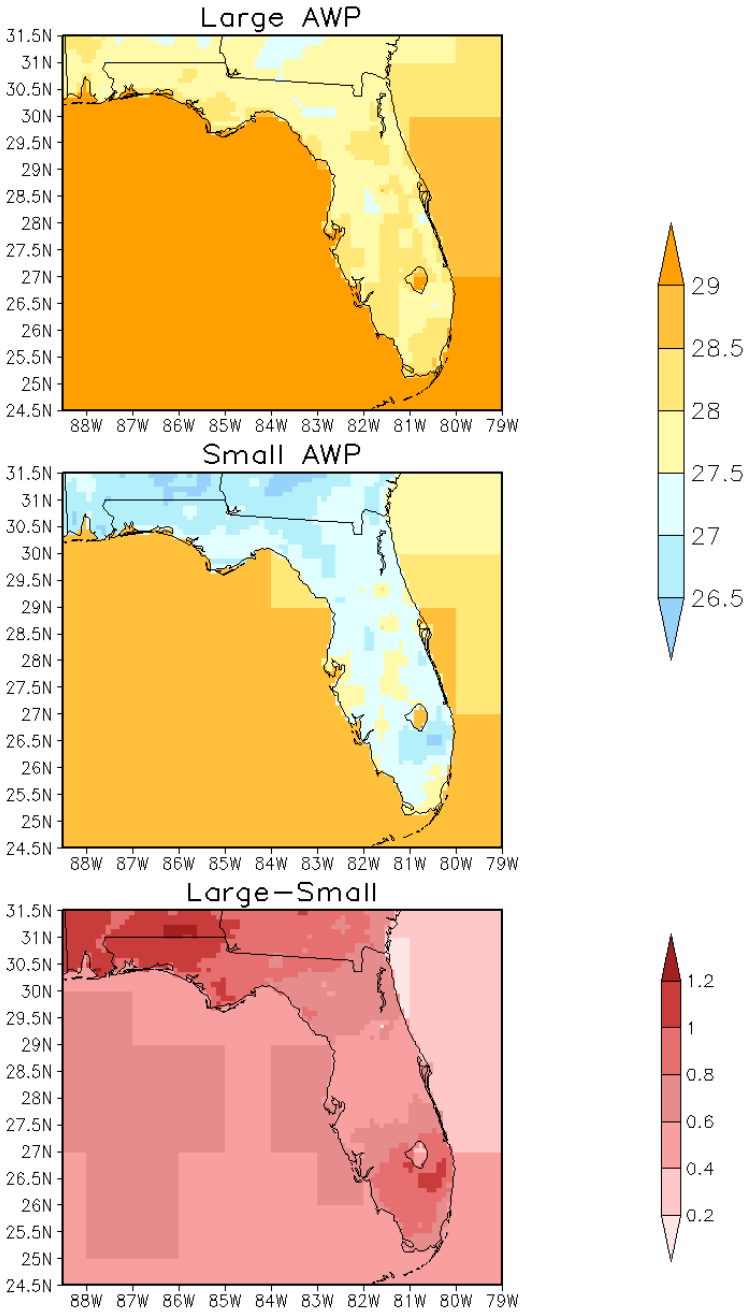

Fig. 3.8. AWP temperature composites. Over land, the shading denotes temperatures from the CLARReS1.0/R2 model integration in units of ˚C, and over the ocean/Gulf of Mexico the shading shows the SST in units of ^{0}C from the ERSSTv3 observational dataset. The panels are (a) the large AWP summer (JJA) composite mean, (b) the small AWP JJA composite mean and (c) the difference (large-small) between the two composite means.

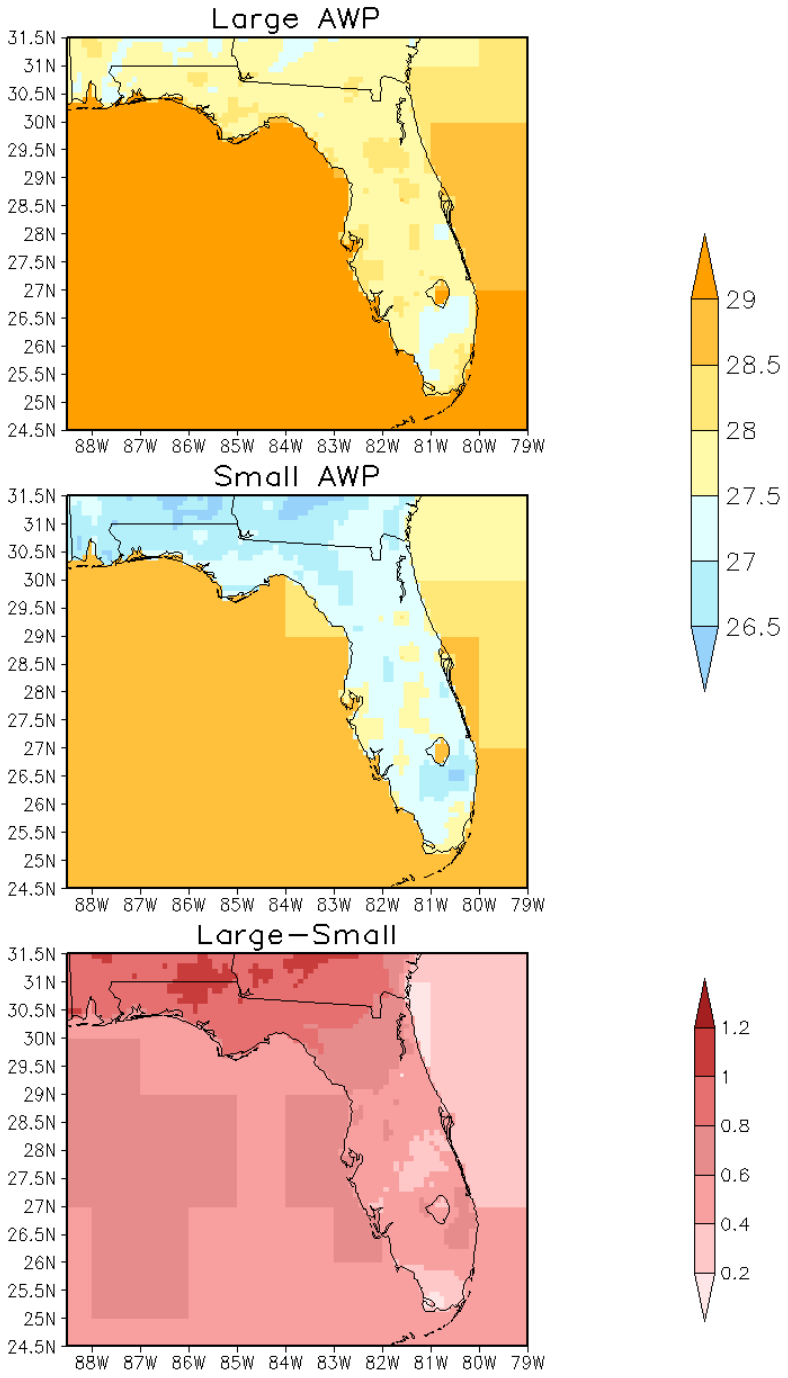

Fig. 3.9. Same as Fig. 3.8 except the data are from the CLARReS1.0/ERA40 model run.

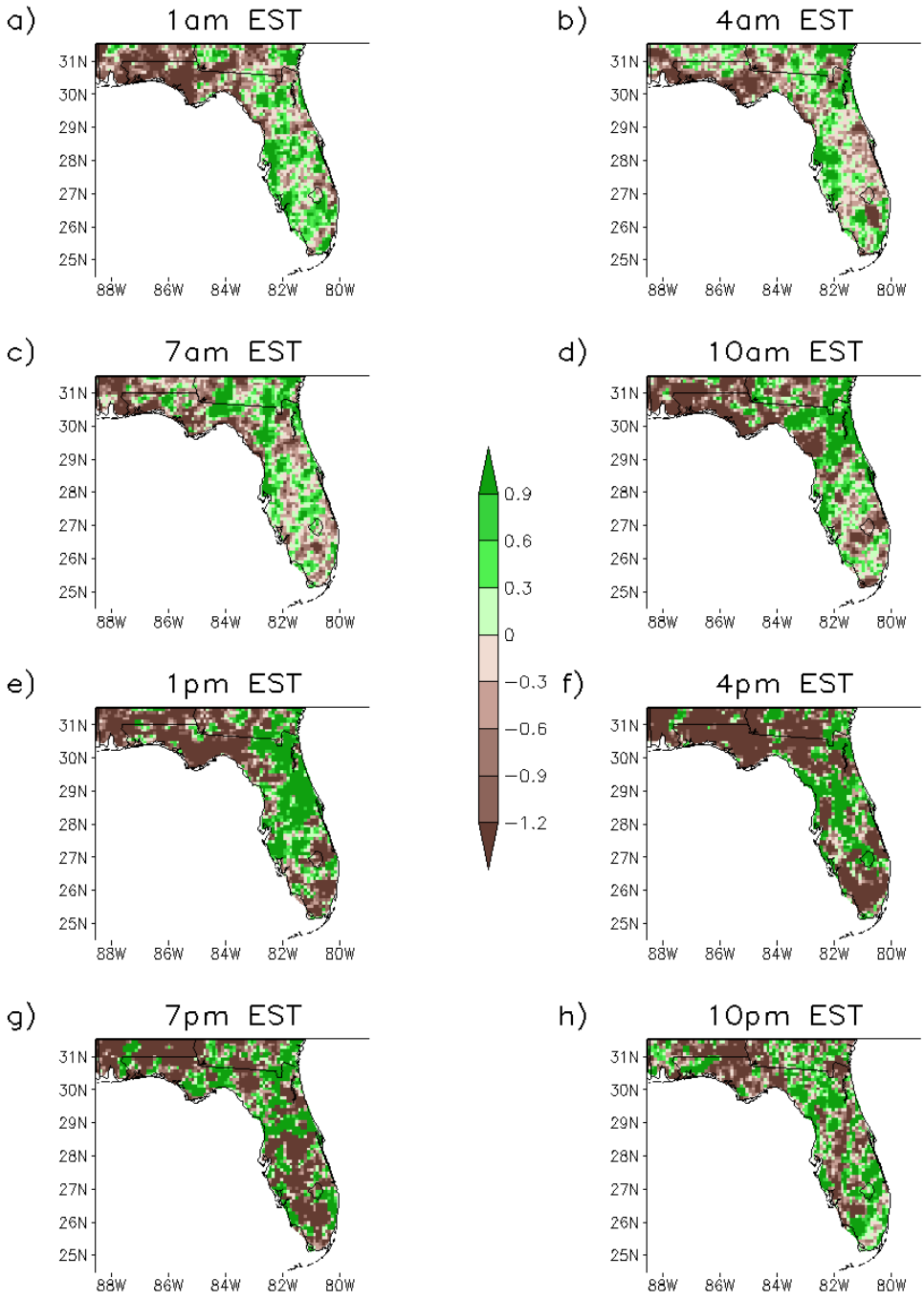

Fig. 3.10. Composite mean differences of precipitation in units of mm day^{-1} from the CLARReS1.0/R2 model run. These composites were averaged at one time (denoted by the panel titles) over JJA from 1979 to 2001 for large and small AWP years, and then the composites were subtracted from each other to obtain the composite mean difference.

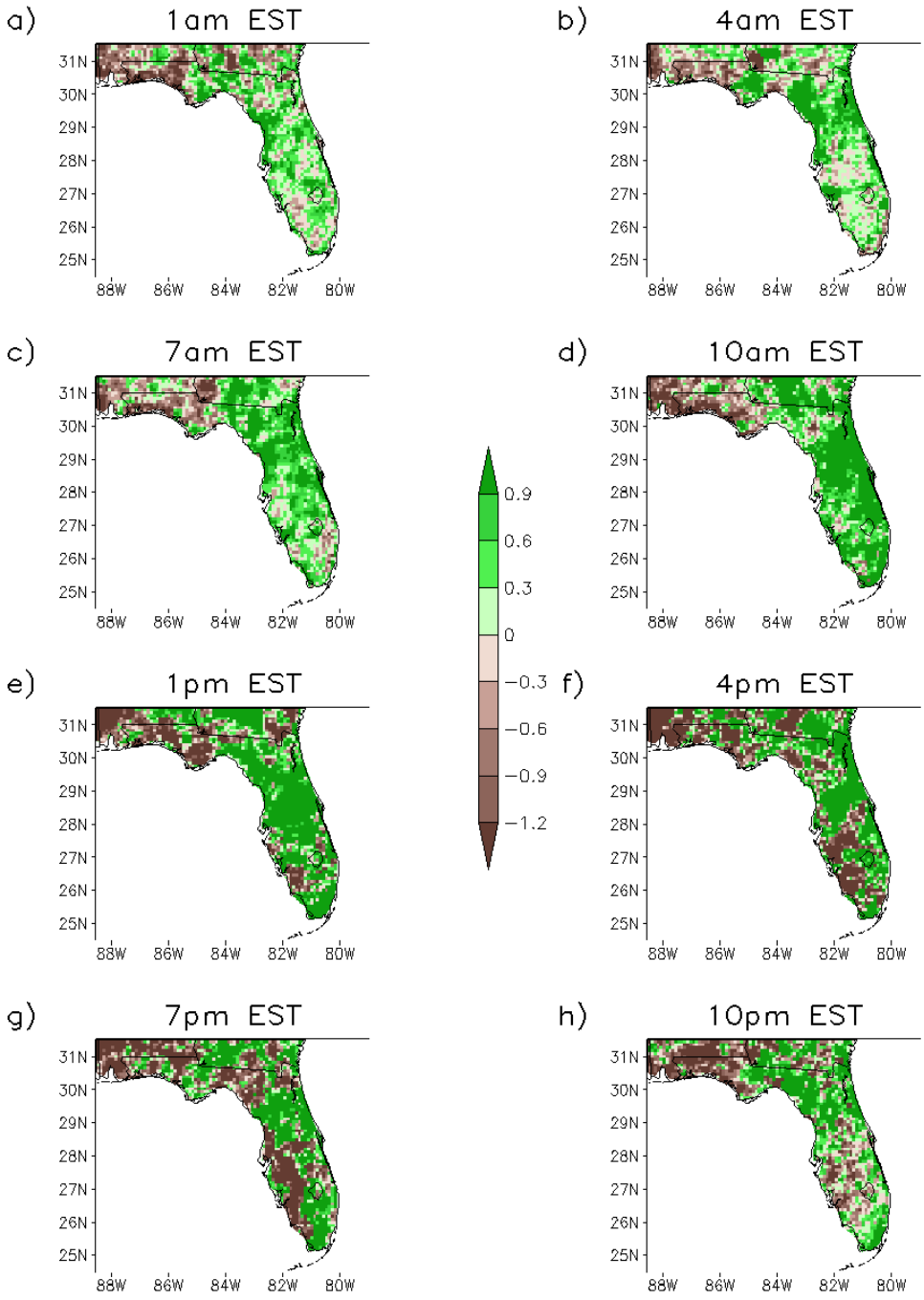

Fig. 3.11. Same as Fig. 3.10 except the data are from the CLARReS1.0/ERA40 model run.

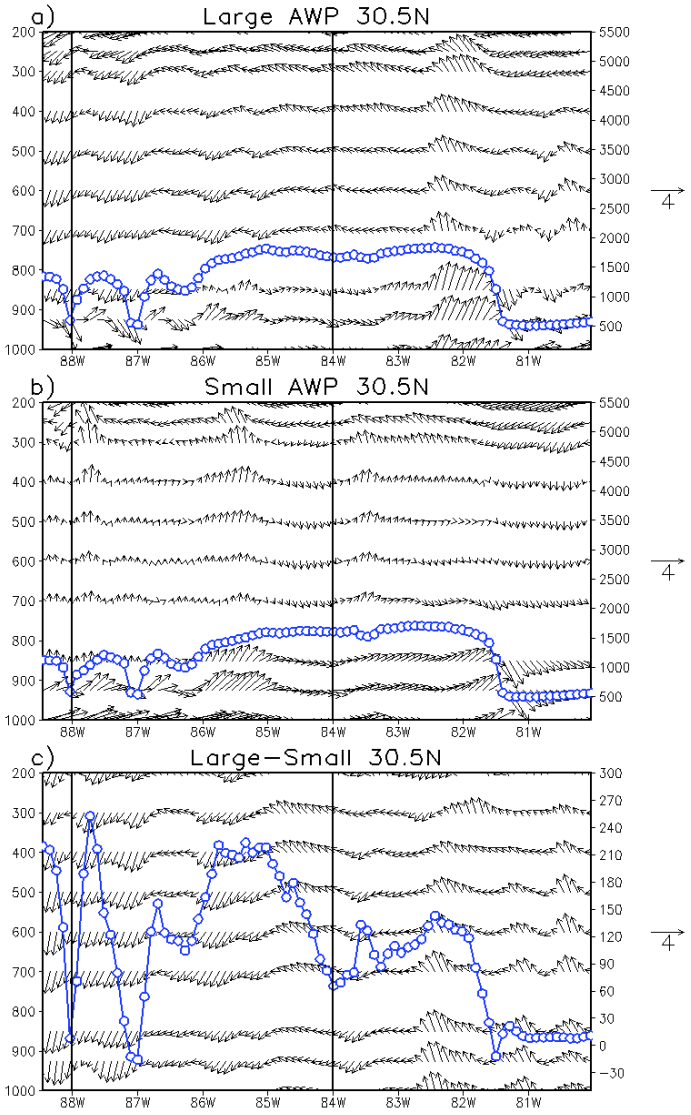

Fig. 3.12. Cross sections through 30.5°N. The vectors indicate the meridional and vertical wind components in units of ms^{-1} taken from the CLARReS1.0/R2 model integration, in which the vertical velocities are scaled by 100. The arrow to the right of each plot gives the vector scale. The left y-axis denotes the height in millibars as a reference to the wind. The blue contour is the planetary boundary layer height from the CLARReS1.0/R2 model integration in meters, which are along the right y-axis. The panels are (a) the large AWP climatological mean composite at 4:00 p.m., (b) the small AWP climatological mean composite at 4:00 p.m. and (c) the difference (large-small) between the 4:00 p.m. composites. The black perpendicular lines mark the locations of 84°W and 88°W.

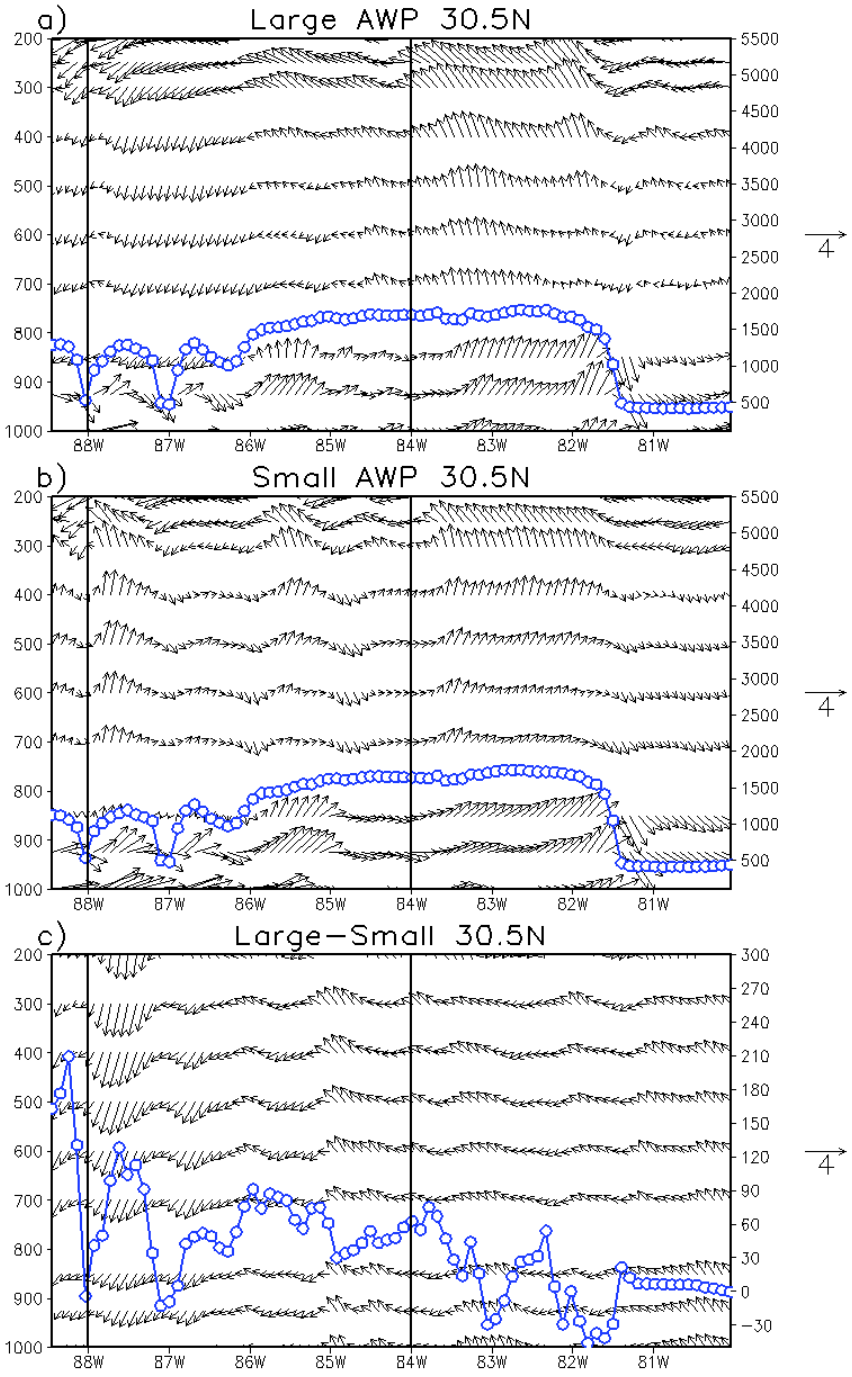

Fig. 3.13. Same as Fig. 3.12 except the variables are from the CLARReS1.0/ERA40 model run.

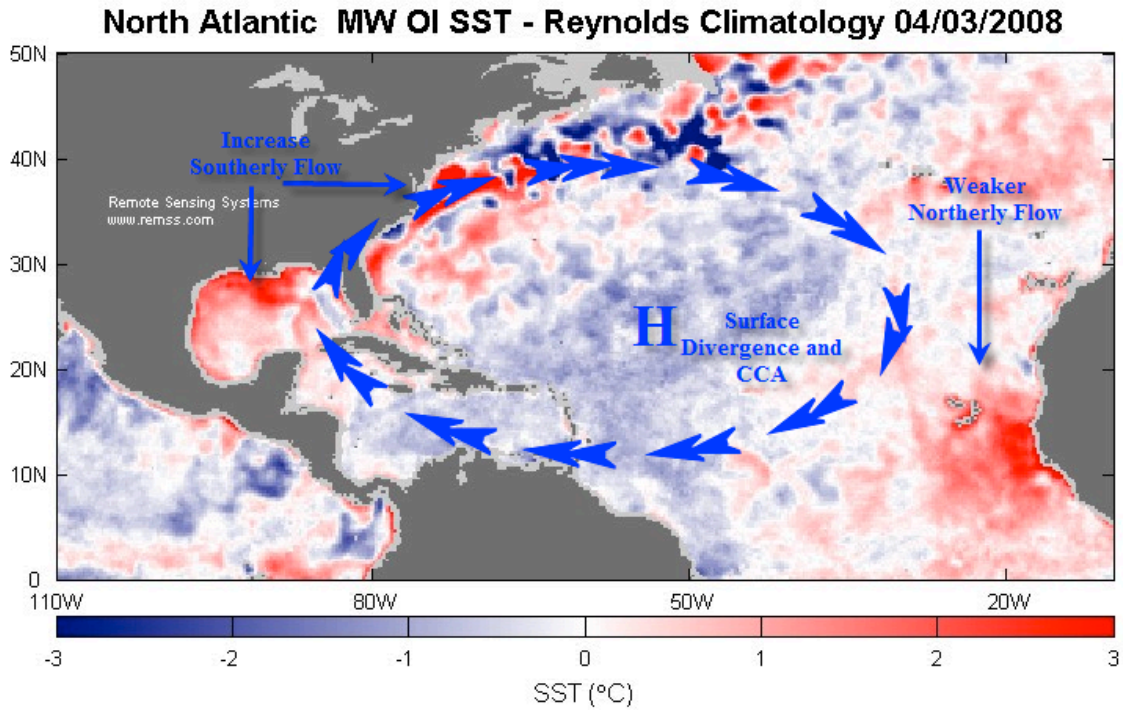

Fig. 3.14. A schematic showing the location of the North Atlantic subtropical high (NASH), from http://talkingmemphis.com/weatherblog/?p=192. The H represents the location of the NASH, and the blue arrowheads denote the flow around the subtropical high. The shaded colors are the SST departures from the Reynolds Climatology using the Microwave Optimally Interpolated product. Information on this product can be found at http://www.ssmi.com/hurricane/active_storms.html#sst.

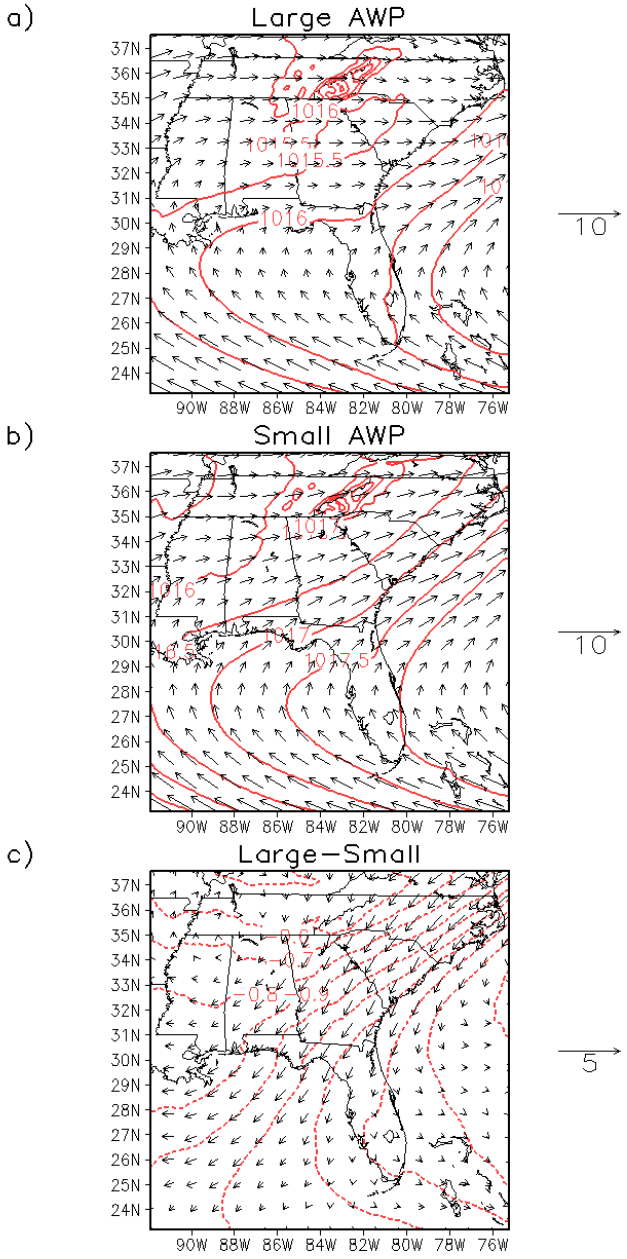

Fig. 3.15. AWP pressure and wind composites. The red contours denote the mean sea level pressure from the CLARReS1.0/R2 model run, in units of mb. The vectors denote the horizontal flow at 850 hPa, also from the CLARReS1.0/R2 model run, in units of ms^{-1} with the scale vector shown by the arrow to the right of the plot. The panels are (a) the large AWP JJA composite mean, (b) the small AWP JJA composite mean and (c) the difference (large-small) between the two composite means.

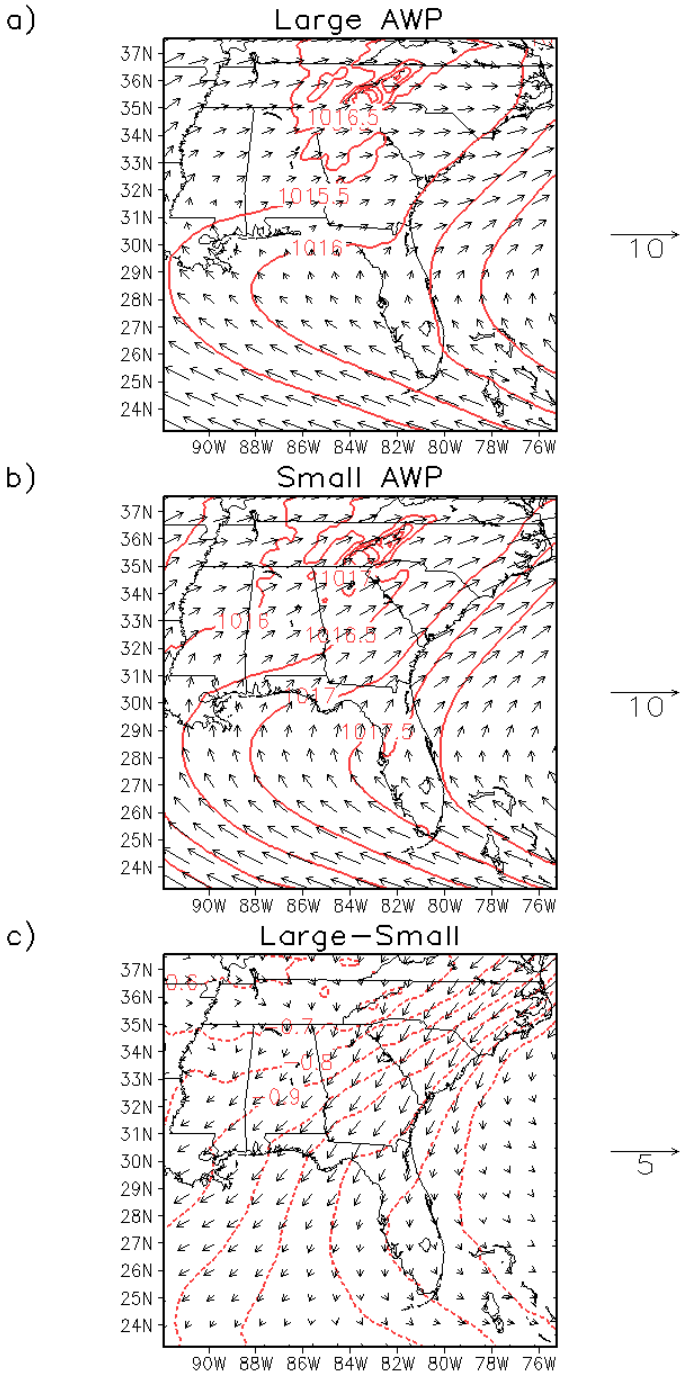

Fig. 3.16. Same as Fig. 3.15 except the variables are from the CLARReS1.0/ERA40 model run.

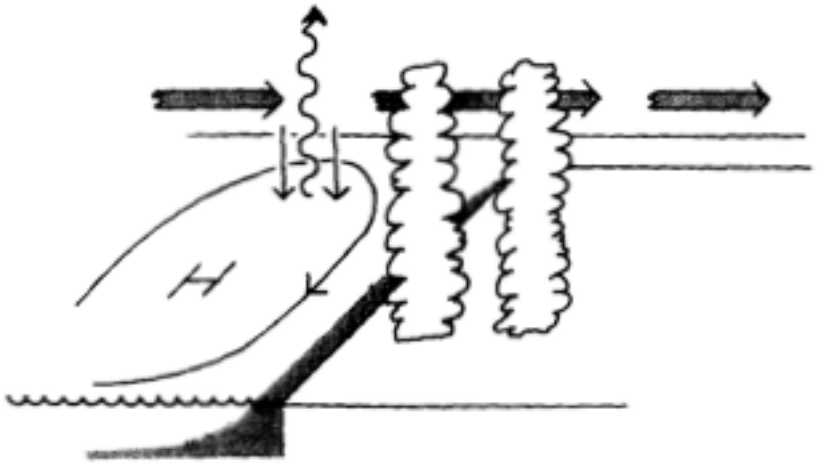

Fig. 3.17. Schematic from Hoskins (1996) showing the Sverdrup vorticity balance at work in relation to the monsoon heating (denoted by puffy clouds), the persistent subtropical high (denoted by H), and flow (denoted by arrows).

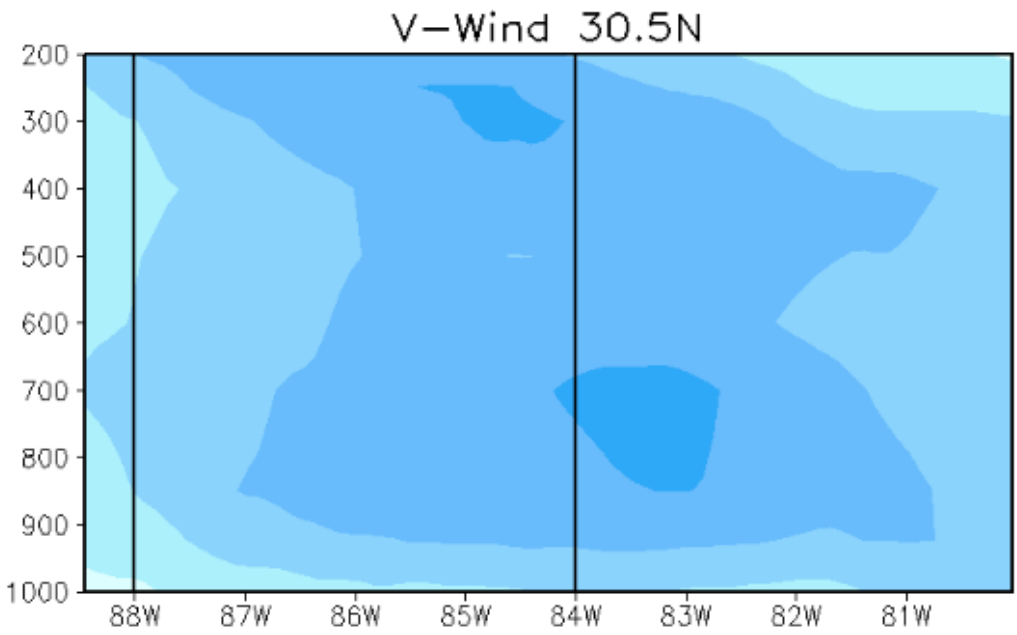

Fig. 3.18. Cross section through 30.5˚N. The black lines on the plot denote the locations of the longitudes 84˚W and 88˚W. The shading is the meridional flow, in which negative values are equatorward flow, in units of ms^{-1}. The wind is from the CLARReS1.0/R2 and is the composite mean difference (large-small) over JJA.

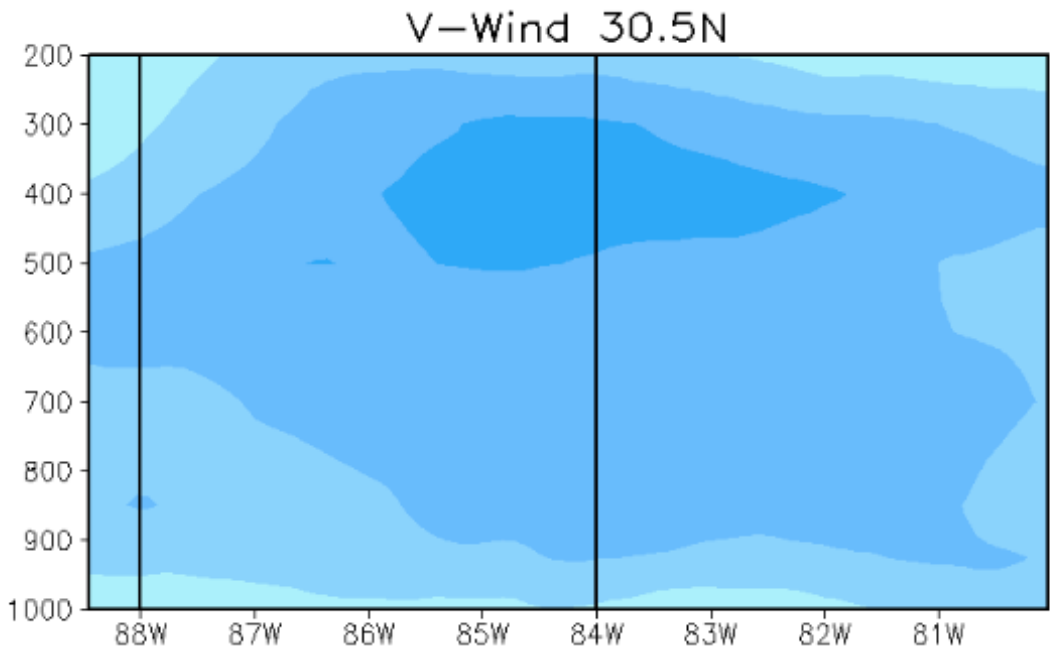

Fig. 3.19. Same as Fig. 3.18 except the data are from the CLARReS1.0/ERA40 model run.

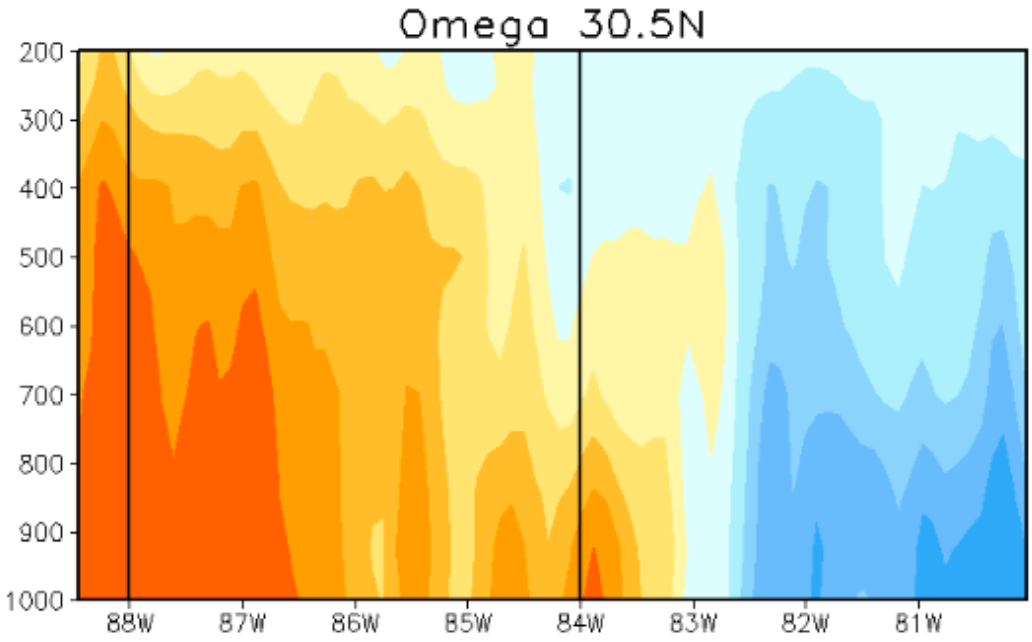

Fig. 3.20. Cross section through 30.5˚N. The black lines on the plot denote the locations of the longitudes 84˚W and 88˚W. The shading is the vertical velocity in Pas^{-1}; the positive values denote sinking motion. Omega is from the CLARReS1.0/R2. This plot is the composite mean difference (large-small) over JJA.

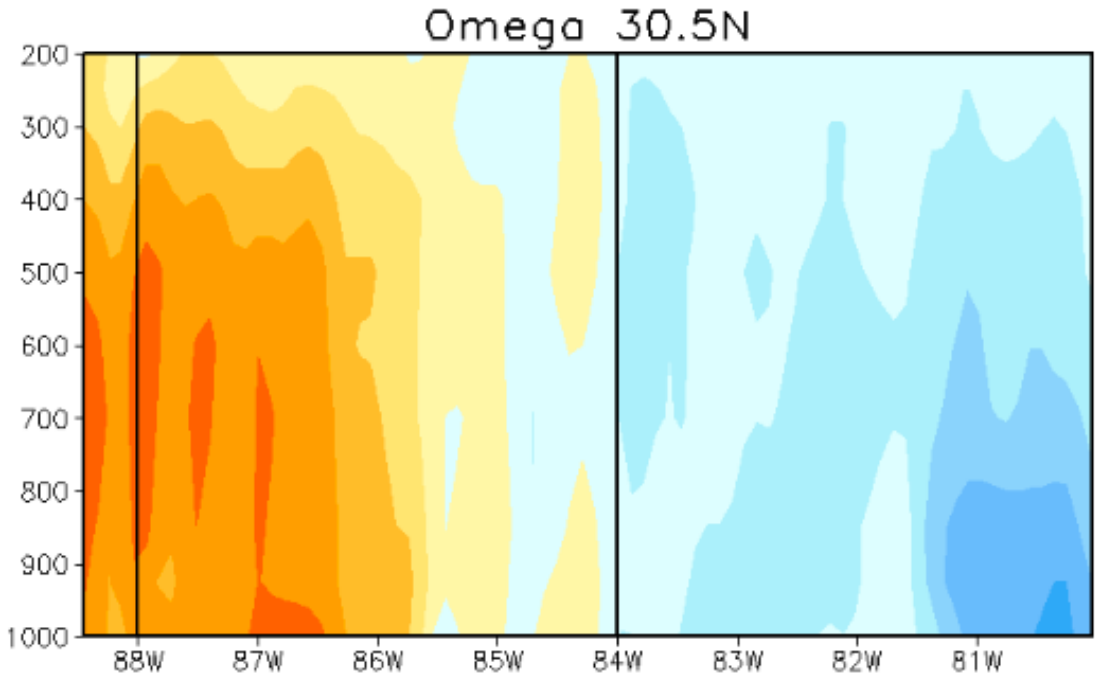

Fig. 3.21. Same as Fig. 3.20 except the data are from the CLARReS1.0/ERA40 model run.

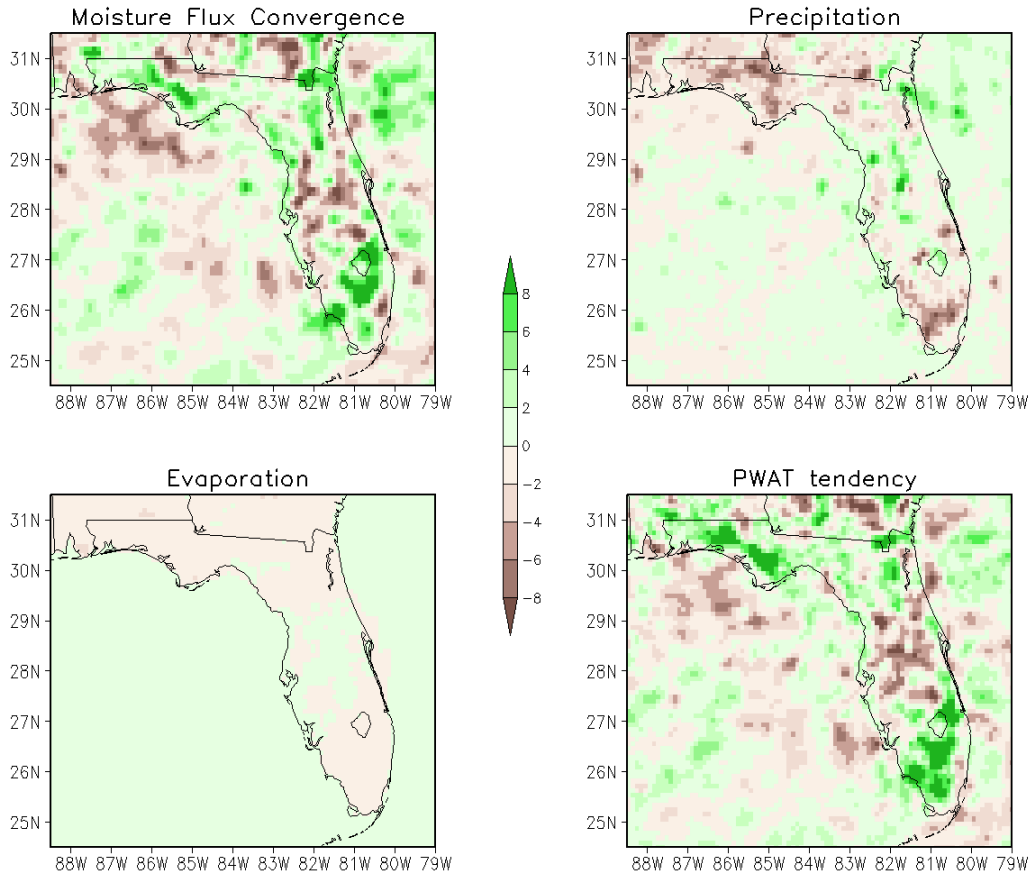

Fig. 3.22. The terms of the moisture budget equations, which are the composite mean difference (large-small) at 4:00 p.m. All are in units of mm day^{-1}. The moisture flux convergence was computed using CLARReS1.0/R2 model run output, precipitation and evaporation are variables from the CLARReS1.0/R2 model output, and the precipitable water tendency is calculated as a residual of these terms.

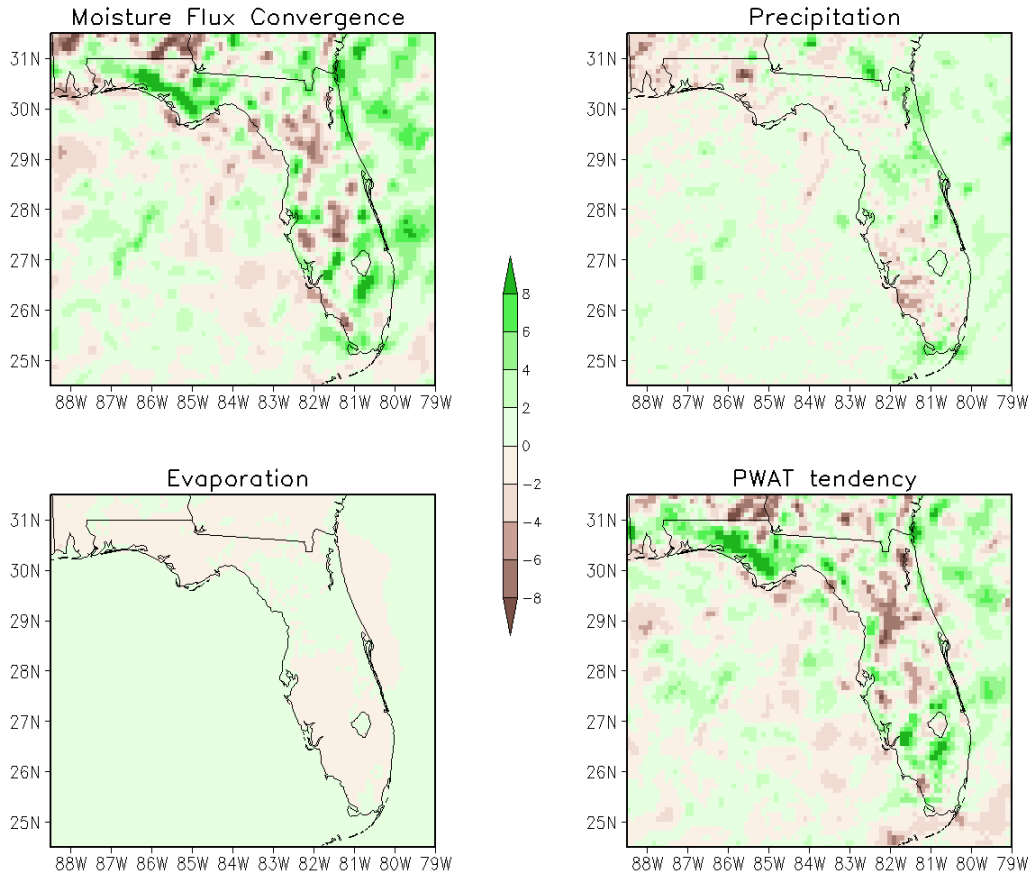

Fig. 3.23. Same as Fig. 3.22 except the variables are from the CLARReS1.0/ERA40 model run.

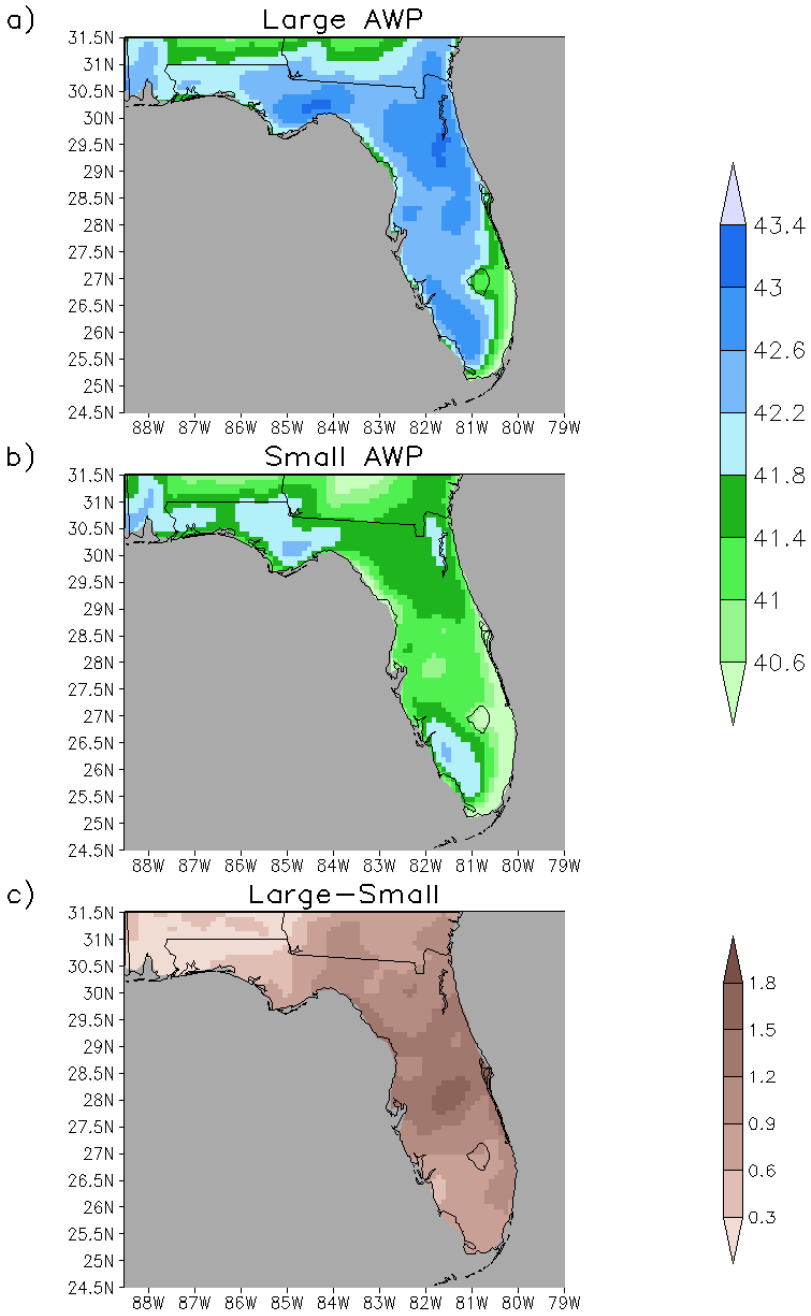

Fig. 3.24. Precipitable water from the CLARReS1.0/R2 model integration for (a) the large AWP JJA composite mean, (b) the small AWP JJA composite mean, and (c) the difference (large-small) between the two composite means. The units are in kgm^{-2}.

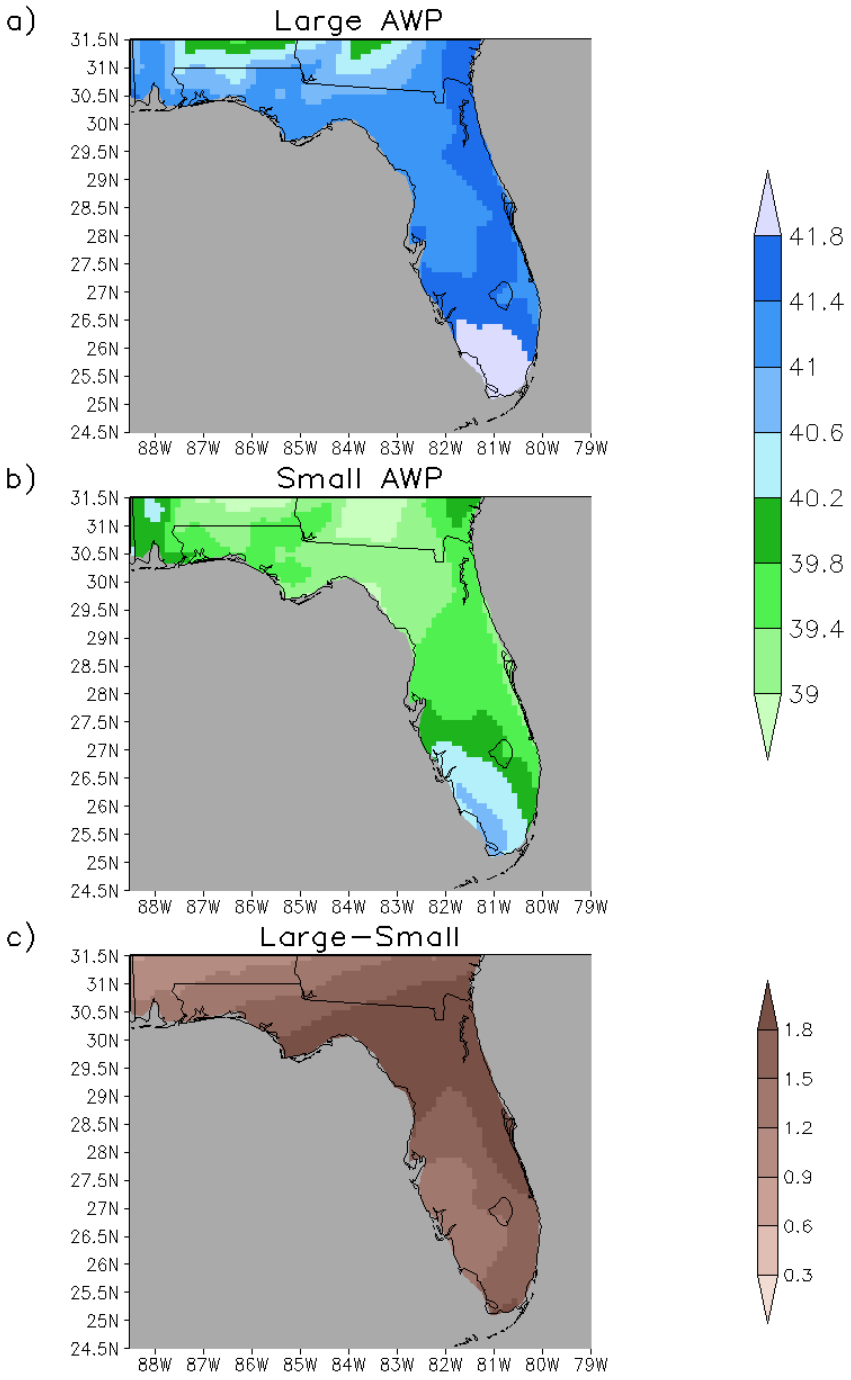

Fig. 3.25. Same as Fig. 3.24 except the data are from the CLARReS1.0/ERA40 model run.

CHAPTER FOUR

CONCLUSIONS

The objective of this study is to determine the low-frequency variations of the sea breeze and convection and to determine the cause of these variations. To accomplish this objective the CLARReS model is integrated twice by downscaling both the R2 and ERA-40 reanalyses with the RSM model provided by NCEP-ECPC. In this downscaling process the lateral boundary conditions are forced with atmospheric variables taken from the reanalyses every six hours. Downscaling yields a product with a much higher resolution (10-km grid spacing) than either previous reanalysis. Both CLARReS model integrations are compared with two validation datasets to check for reliability. The NCEP-EMC precipitation estimates are available hourly; on the other hand, the CPC precipitation is only available daily. Thus, the NCEP-EMC precipitation is used specifically for the diurnal climatological mean of the precipitation over Florida, and the CPC precipitation is used to check the validity of the interannual output. On the diurnal scale both the CLARReS1.0/R2 and the CLARReS1.0/ERA40 correctly simulate the times the maximum and minimum precipitation (4:00 p.m. and 4:00 a.m., respectively) occurred. The maximum vertical motions are also reproduced at this time. However, both runs underestimate the amount of precipitation occurring climatologically, the CLARReS1.0/R2 more so than the CLARReS1.0/ERA40. Observations show that precipitation is weaker over most of Florida for large AWP years than it is for small AWP years. The CLARReS1.0/R2 correctly simulates this pattern on an interannual time scale over the panhandle of Florida west of 84°W, but the CLARReS1.0/ERA40 does not pick up this interannual signal until 86°W. Neither model run reproduces the interannual variations found in the observations over peninsular Florida because of the more complicated nature of the sea breeze over this region.

The reasons for this interannual signal are further investigated. Both models are in agreement in suggesting that the temperature gradient between the panhandle of Florida and the Gulf of Mexico is higher for large AWP years than for small years, even though less precipitation occurs for large AWP years. However, because the precipitation patterns at 4:00 p.m. match the composite difference, there is strong suggestion in the model that the sea breeze is modulated interannually. This modulation comes from changes to the intensity and location of

the NASH, which varies interannually with the AWP. During large AWP years, the NASH weakens and is located farther east than it is in small AWP years. This in turn induces an anomalous equatorward flow over the panhandle of Florida; large-scale subsidence occurs for large AWP years as dictated by the Sverdrup vorticity balance. This mechanism is shown in a schematic (Fig. 4.1), and the opposite effect for small AWP years is illustrated in Fig. 4.2.

Finally, the moisture budget equation is examined to resolve the issue of finding stronger circulations during large AWP years despite the lack of convection. The moisture flux convergence is stronger for large AWP years over the panhandle of Florida, although the exact reasons for this are unknown. However, after each component of the moisture budget equation is plotted, the precipitable water is shown to increase for large AWP years when calculated as a residual. This is confirmed in the model output as well. Therefore, the atmospheric column experiences greater moisture accumulation for large AWP years since it is unable to precipitate out of the column as a result of large-scale subsidence.

Combined, these results indicate that low-frequency variations of the convection and subsequently the sea breeze exist for panhandle Florida because of the variations of the AWP. These deviations in interannual precipitation occur because the NASH changes location and intensity, which in turn changes the large-scale flow over the southeast United States. However, these results are restricted to the Florida panhandle. The model integrations are not able to correctly simulate the interannual signal over peninsular and northeast Florida, and at this time the interannual signal for this region is not understood. The entire state of Florida will again be considered in future work in which the effects of land use land cover on sea breeze over the model temporal domain will be examined.

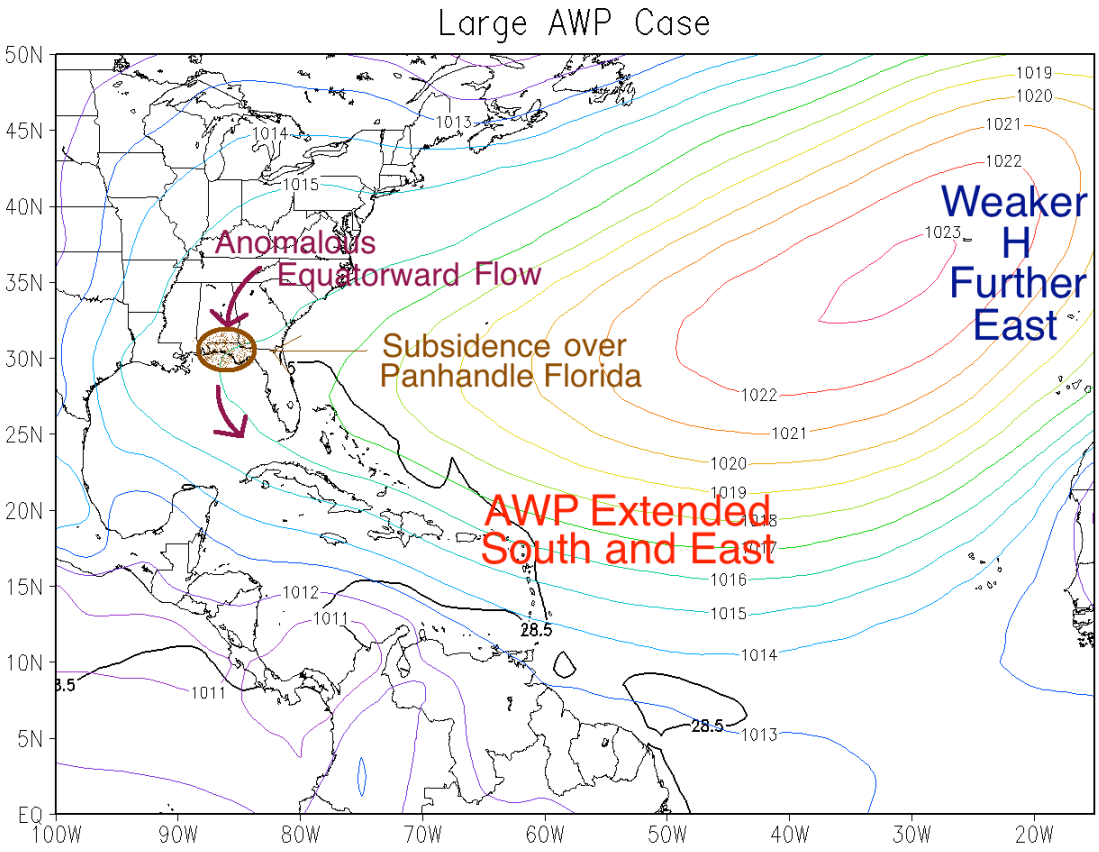

Fig. 4.1. Schematic showing the AWP effects on the low-frequency variance of the panhandle Florida sea breeze for the large AWP case. The rainbow contour lines are mean sea level pressure in mb. The black contour line denotes the 28.5°C SST isotherm. The maroon arrows depicts the anomalous meridional flow over the southeast United States, and the area of brown stippling shows the area of subsidence.

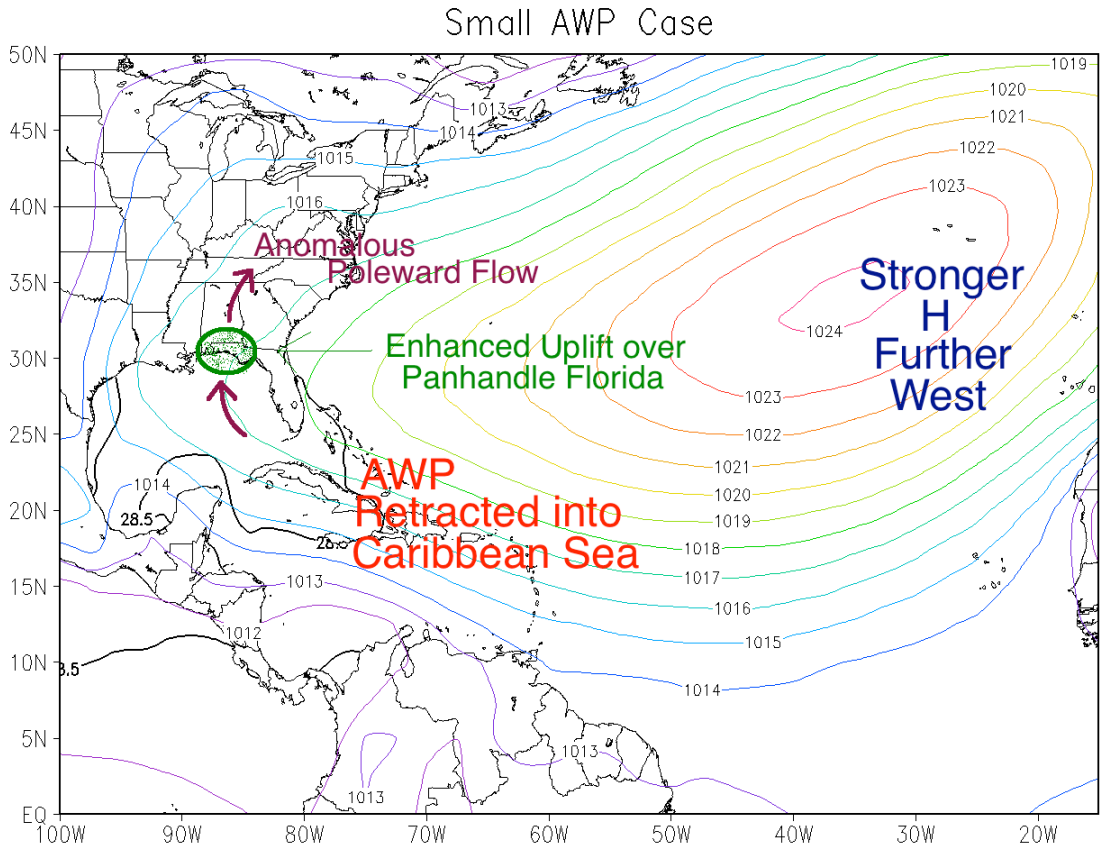

Fig. 4.2. Schematic showing the AWP effects on the low-frequency variance of the panhandle Florida sea breeze for the small AWP case. The rainbow contour lines are mean sea level pressure in mb. The black contour line denotes the 28.5°C SST isotherm. The maroon arrows depicts the anomalous meridional flow over the southeast United States, and the area of green stippling shows the area of enhanced uplift.

REFERENCES

Arritt, R.W., 1993: Effects of the large-scale flow on characteristic features of the sea breeze. *J. Appl. Meteor.*, 32, 116-125.

Biggs, W.G., and M.E. Graves, 1962: A lake breeze index. *J. Appl. Meteor.*, 1, 474-480.

Carter, L.M., 2003: US National Assessment of the Potential Consequences of Climate Variability and Change Educations Resources Regional Paper: The Southeast. Available online at www.usgcrp.gov/usgcrp/nacc/education/southeast/se-edu-3.htm

Chou, M.D. and M. J. Suarez, 1994: An efficient thermal infrared radiation parameterization for use in General Circulation Models. Technical Report Series on Global Modeling and Data Assimilation, National Aeronautical and Space Administration/TM-1994-104606, 3, 85 pp.

Chou, M.D., and K.T. Lee, 1996: Parameterizations for the Absorption of Solar Radiation by Water Vapor and Ozone. J. Atmos. Sci., 53, 1203–1208.

Ek, M. B., K. E. Mitchell, Y. Lin, E. Rogers, P. Grunmann, V. Koren, G. Gayno, and J. D. Tarpley (2003), Implementation of Noah land surface model advances in the National Centers for Environmental Prediction operational mesoscale Eta model, J. Geophys. Res., 108, D228851, doi:10.1029/2002JD003296

Estoque, M.A., 1962: The sea breeze as a function of the prevailing synoptic situation. *J. Atmos. Sci.*, 19, 244-250.

Fuelberg, H.E., and D.G. Biggar, 1994: The preconvective environment of summer thunderstorms over the Florida panhandle. *Weather and Forecasting*, 9, 316-326.

Higgins, R. W., W. Shi, E. Yarosh, and R. Joyce, 2000: Improved United States Precipitation Quality Control System and Analysis. NCEP/Climate Prediction Center Atlas 7, NOAA, 40pp.

Hong, S.Y., and H.L. Pan, 1996: Nonlocal Boundary Layer Vertical Diffusion in a Medium-Range Forecast Model. Mon. Wea. Rev., 124, 2322–2339.

Hoskins, B. (1996): On the existence and strength of the summer subtropical anticyclones, *Bull. Amer. Meteor. Sac.,* 77: 1287-1292.

Hsu, S-A., 1970: Coastal air-circulation system: Observations and empirical model. *Monthly Weather Review*, 98, 487-509.

Juang, H. H., and M. Kanamitsu, 1994: The NMC Nested Regional Spectral Model. Mon. Wea. Rev. 122, 3-26.

Kanamaru, H., and M. Kanamitsu, 2007: Scale-selective bias correction in a downscaling of global analysis using a regional model. *Mon. Wea. Rev.*, **135,** 334–350

Kanamitsu, M., W. Ebisuzaki, J. Woolen, S. K. Yang, J. J. Hnilo, M. Fiorino and J. Potter, 2002: NCEP/DOE AMIP-II Reanalysis (R-2). Bull. Amer. Met. Soc. 83, 1631-1643. DOI: 10.1175/BAMS-83-11-163

Li, W., L. Li, R. Fu, Y. Deng, and H. Wang, 2011: Changes to the North Atlantic Subtropical High and Its Role in the Intensification of Summer Rainfall Variability in the Southeastern United States. *Mon. Wea. Rev.,* under review

Lim, Y.-K., L. B. Stefanova, S. C. Chan, S. D. Schubert, and J. J. O'Brien, 2010: High-resolution subtropical summer precipitation derived from dynamical downscaling of the NCEP/DOE reanalysis: How much small-scale information is added by a regional model? Clim Dyn., doi: 10.1007/s00382-010-0891-2.

Lin, Y., and K. E. Mitchell, 2005: The NCEP stage II/IV hourly precipitation analyses: development and applications. Preprints, 19th Conf. on Hydrology, American Meteorological Society, San Diego, CA, 9-13 January, Paper 1.2.

Lopez, R.E., P.T. Gannon Sr, D.O. Blanchard, and C.C. Balch, 1984: Synoptic and regional circulation parameters associated with a degree of convective shower activity in south Florida. *Monthly Weather Review*, 112, 686-703.

Loveland, T. R., Merchant, J. W., Reed, B. C., Brown, J. F., Ohlen, D. O., Olson, P., and Hutchinson, J., 1995, Seasonal land cover regions of the United States. Annals of the Association of American Geographers, 85, 339–355.

Mak, K-M, and J.E. Walsh, 1976: On the relative intensities of sea and land breezes. *J. Atmos. Sci.*, 33, 242-251.

Miller, S.K. and B.D. Keim, 2003: Synoptic-scale controls on the sea breeze of the central New England coast. *Weather and Forecasting*, 18, 2, 236-248.

Neumann, J. and Y. Mahrer, 1971: A theoretical study of the land and sea breeze circulation. *J. Atmos. Sci.*, 28, 532-542.

Pan, H.-L., and W.-S. Wu, 1994: Implementing a mass-flux convective parameterization package for the NMC Medium Range Forecast Model. Preprints, 10th Conf. on Numerical Weather Prediction, Portland, OR, Amer. Meteor. Soc., 96–98

Pielke, R.A., 1974: A three-dimensional numerical model of the sea-breeze over south Florida. *Monthly Weather Review*, 102, 115-139.

Powell, M. D., and S. K. Rinard, 1998: Marine forecasting at the 1996 centennial Olympic Games. *Wea. Forecasting*, **13,** 764–782.

Rodwell, M. J., and B. J. Hoskins, 2001: Subtropical anticyclones and summer monsoons. J. Climate, 14, 3192–3211.

Simpson, J.E., 1994: Sea Breeze and Local Winds. Cambridge Univ Press, 234 pp.

Slingo, J. M., 1987: The development and verification of a cloud prediction scheme for the ECMWF model. *Quart. J. Roy. Meteor. Soc.,***113,** 899–927

Smith, T. M., R. W. Reynolds, T. C. Peterson, and J. Lawrimore, 2008: Improvements to NOAA's historical merged land-ocean surface temperature analysis (1880-2006). J. Climate, 21, 2283-2296.

Stefanova, L., V. Misra, S. C. Chan, M. Griffin, J. J. O'Brien, and T. J. Smith III, 2011: A proxy for high-resolution regional reanalysis for the Southeast United States. Clim Dyn, under review

Uppala, S. M., and Coauthors, 2005: The ERA-40 reanalysis. *Quart. J. Roy. Meteor. Soc.*, **131,** 2961–3012.

Wang, C. and D. B. Enfield, 2001: The tropical western hemisphere warm pool. Geophys. Res. Lett., 28, 1635-1638.

——, D. B. Enfield, S.-K. Lee, and C. W. Landsea, 2006: Influences of the Atlantic warm pool on Western Hemisphere summer rainfall and Atlantic hurricanes. J. Climate, 19, 3011–3028.

——, and S.-K. Lee, 2007: Atlantic warm pool, Caribbean low- level jet, and their potential impact on Atlantic hurricanes. Geophys. Res. Lett., 34, L02703, doi:10.1029/2006GL028579.

——, S.-K. Lee, and D. B. Enfield, 2008: Climate response to anomalously large and small Atlantic warm pools during the summer. J. Climate, 21, 2437–2450.

Zhou, T., and Coauthors, 2009: Why the western Pacific subtropical high has extended westward since the late 1970s. *J. Climate*, **22,** 2199–2215.

BIOGRAPHICAL SKETCH

Lauren Moeller was born in Washington, Missouri, in 1987. She grew up in a small town on the outskirts of the St. Louis Metropolitan area. When she was 10 her house was hit by a tornado, and at that point she began reading zealously on all types of severe weather phenomenon. This interest led to a decision to pursue meteorology as a career.

After graduating from Warren County R-III, she went to University of Missouri to pursue a Bachelor of Science degree in 2005. While there, Lauren pursued many extracurricular activities. She was a member of the Mizzou Storm Chase team all four years, experiencing three chases. Lauren was also deeply involved in the school's chapter of the AMS/NWA association, and became the first president of the newly established Chi Epsilon Pi Mizzou chapter. Through Chi Epsilon Pi, a tutoring program was started in order to help incoming undergraduates with the course load expected of a meteorology student. Lauren received a research scholarship in 2008, which allowed her to conduct research under the advisement of Dr. Neil Fox. Her topic of research involved the effects of a tree line on evaporation over crop fields. She presented her work in multiple conferences.

Lauren received a Bachelor of Science in Soil, Environmental, and Atmospheric Science in the spring of 2009. She enrolled into Florida State University in fall of 2009 to pursue a Master of Science under the advisement of Dr. Vasubandhu Misra and Dr. James J. O'Brien. She was an active member of the North Florida chapter of the AMS, and won the Member of the Year award for the 2009-2010 year. Lauren was also active in the outreach programs in place at the Center for Oceanic-Atmospheric Prediction Studies, in which she visited elementary and middle school students to teach about weather hazards. She is thankful for all the opportunities given to her at Florida State, and has enjoyed her time there.